OAK RIDGE
NATIONAL LABORATORY

MANAGED BY UT-BATTELLE
FOR THE DEPARTMENT OF ENERGY

UT–BATTELLE

Results from ORNL Characterization of ZrO2-500-AK2 – Surrogate TRISO Material

Andrew K. Kercher and John D. Hunn

Oak Ridge National Laboratory

This document is a compilation of the characterization data for the TRISO-coated surrogate particles designated ZrO2-500-AK2 that was produced at Oak Ridge National Laboratory (ORNL) as part of the Advanced Gas Reactor Fuel Development and Qualification (AGR) program. The ZrO2-500-AK2 material contains nominally 500 μm kernels of yttria-stabilized zirconia (YSZ) coated with all TRISO layers (buffer, inner pyrocarbon, silicon carbide, and outer pyrocarbon). The ZrO2-500-AK2 material was created for: (1) irradiation testing in the High Flux Isotope Reactor (HFIR) and (2) limited dissemination to laboratories as deemed appropriate to the AGR program. This material was created midway into a TRISO fuel development program to accommodate a sudden opportunity to perform irradiation testing on surrogate material. While the layer deposition processes were chosen based on the best technical understanding at the time, technical progress at ORNL has led to an evolution in the perceived optimal deposition conditions since the creation of ZrO2-500-AK2. Thus, ZrO2-500-AK2 contains a reasonable TRISO microstructure, but does differ significantly from currently produced TRISO surrogates and fuel at ORNL. In this document, characterization data of the ZrO2-500-AK2 surrogate includes: size, shape, coating thickness, and density.

For comparison purposes, some data pertaining to a German reference fuel have been included in this report. The German reference fuel was a sample of the EUO 2358-2365 composite studied by General Atomics (GA) and referenced in GA document #910852 "Acceptance Test Report for German Fuel Particles."

Table of Contents

1   Processing Conditions

R.A. Lowden, J.H. Miller

The ZrO2-500-AK2 kernels were ~0.5 mm YSZ (yttria-stabilized zirconia) grinding media sold by the TOSOH Corporation and manufactured by the Nikkato Corporation. The lot number for the YSZ grinding media was #5230460050. The following information was measured by the manufacturer and reported in the inspection sheet associated with this specific lot: density 6.04 g/cm^3, hardness (HV1) 12.7 GPa, and crushing load 0.22 kN.

Kernels were coated with the different TRISO layers by chemical vapor deposition (CVD) in a fluidized bed furnace. The fluidized bed furnace had a 2" diameter tube and a 0.125" gas inlet diameter. The precursor loading for the coating run for ZrO2-500-AK2 included 55 grams of YSZ kernels and also 0.8 grams of small rods (which were produced for other studies). The kernels were fluidized in argon, and the furnace was heated to 1250°C. Once stabilized at 1250°C, buffer carbon was deposited for 5 minutes under a flow of 3.9 L/min acetylene and 2.6 L/min argon. After buffer deposition, the furnace was purged in argon under fluidizing conditions. Then, the inner pyrocarbon (IPyC) was deposited at 1250°C for 9 minutes under a flow of 1.05 L/min acetylene, 1.05 L/min propylene, and 4.9 L/min argon. After IPyC deposition, the furnace was purged in argon under fluidizing conditions while heating up to 1400°C. Silicon carbide was deposited at 1400°C for 145 minutes using precursors of hydrogen and methyl trichlorosilane (MTS), which is a liquid precursor. A bubbler with a 0.5 L/min carrier stream of hydrogen was used to introduce MTS into the gas flow at an approximate mass flow rate of 0.008 g/min. The gas flows for SiC deposition were 4.75 L/min hydrogen (including bubbler carrier stream) and 4.25 L/min argon. The furnace was cooled down to 1250°C in argon under fluidizing conditions. The outer pyrocarbon (OPyC) was deposited for 8 minutes under a flow of 1.275 L/min acetylene, 1.275 L/min propylene, and 5.95 L/min argon. Then, the furnace was cooled to room temperature in argon under fluidizing conditions. The final weight of TRISO surrogate particles was about 140 grams.

2   Coating Fractography

J.D. Hunn and N. Hashimoto

A ZrO2-500-AK2 particle was crushed to fracture in order to examine the fracture surfaces. Since analysis was performed on a single particle, no claims can be made on the statistical relevance of these results. Nonetheless, it is believed that these images should be representative of fracture surfaces of ZrO2-500-AK2 particles. The coatings separated cleanly from the kernel. A large fragment was identified for SEM analysis in secondary electron and backscatter modes. All of the coatings remained attached to each other in the fragment (Figure 2-1), but extensive interfacial cracking was observed at the SiC/OPyC boundary (Figure 2-5).

The buffer fracture surface was highly jagged; the fracture likely propagated predominantly through high porosity regions of the buffer (Figure 2-2). The fracture surfaces of the other layers are significantly more uniform. The IPyC and OPyC were deposited under similar conditions,

and thus they had similar fracture surfaces (Figure 2-3). The IPyC fracture surface (Figure 2-4) and OPyC fracture surface (Figure 2-5) showed evidence of a nodular microstructure. Pyrocarbon deposition can occur by: (1) direct deposition onto the surface and/or (2) gas phase nucleation of carbon and subsequent deposition of the carbon nuclei onto the surface. For both the IPyC and OPyC, the presence of a nodular microstructure indicates that a significant amount of pyrocarbon deposition occurred by gas phase nucleation and subsequent deposition.

The IPyC/SiC interface exhibited extensive interlacing (Figure 2-4), but the OPyC/SiC interface had no apparent interlacing and poor interfacial strength (Figure 2-5). A crack inside the particle demonstrated extensive propagation along the OPyC/SiC interface (possibly exfoliation). During processing, the SiC deposited onto a nodular IPyC surface, which likely caused the extensive interlacing at the IPyC/SiC interface, whereas the OPyC deposited onto a relatively smooth SiC surface, which likely caused the abrupt transition at the OPyC/SiC interface.

Unlike the buffer, IPyC, and OPyC layers, the SiC layer did not fracture predominantly along microstructural features. The SiC fracture surface suggested a combination of intergranular and intragranular fracture (Figure 2-6). Stepped fracture surfaces, which indicate intragranular fracture, occurred in small regions. The localized nature of intragranular fracture suggested that intergranular fracture was a significant fracture mode. In comparison, the German reference fuel (Figure 2-7) had intragranular fracture that extended over longer distances, which would suggest that intergranular fracture was less significant in the German reference fuel than in the ZrO2-500-AK2 (given their similar grain size; see section 7.2).
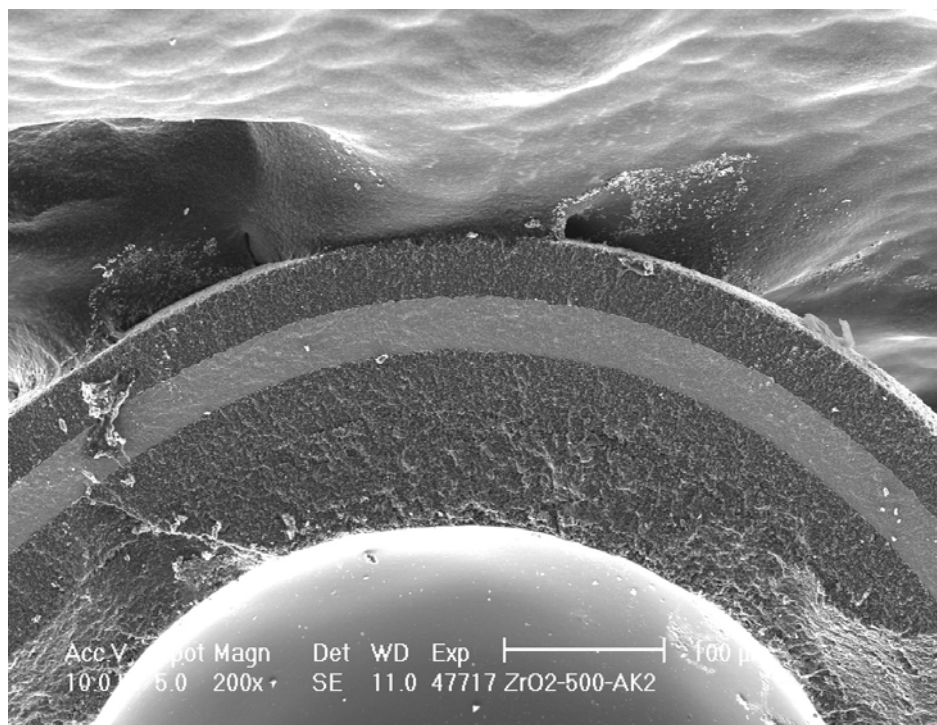
Figure 2-1: Fracture surface of ZrO2-500-AK2 showing buffer, IPyC, SiC, and OPyC. (SEM, secondary electron mode)
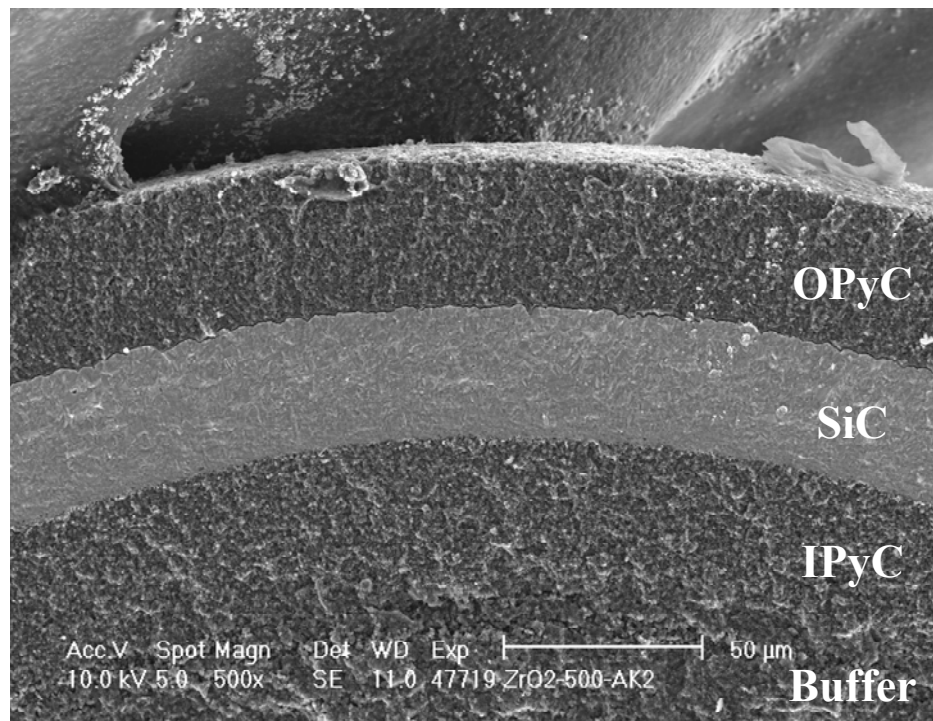
Figure 2-2: A comparison of fracture surfaces shows the high roughness of the buffer fracture surface (bottom) relative to the other fracture surfaces (SEM, secondary electron).
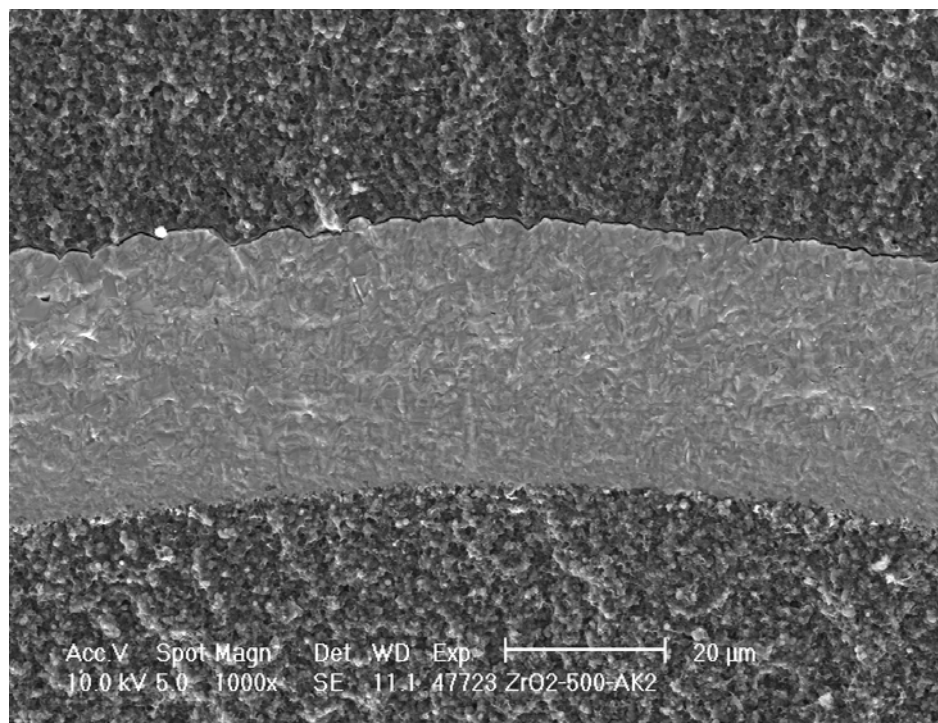
Figure 2-3: IPyC, SiC, and OPyC fracture surfaces (SEM, secondary electron).
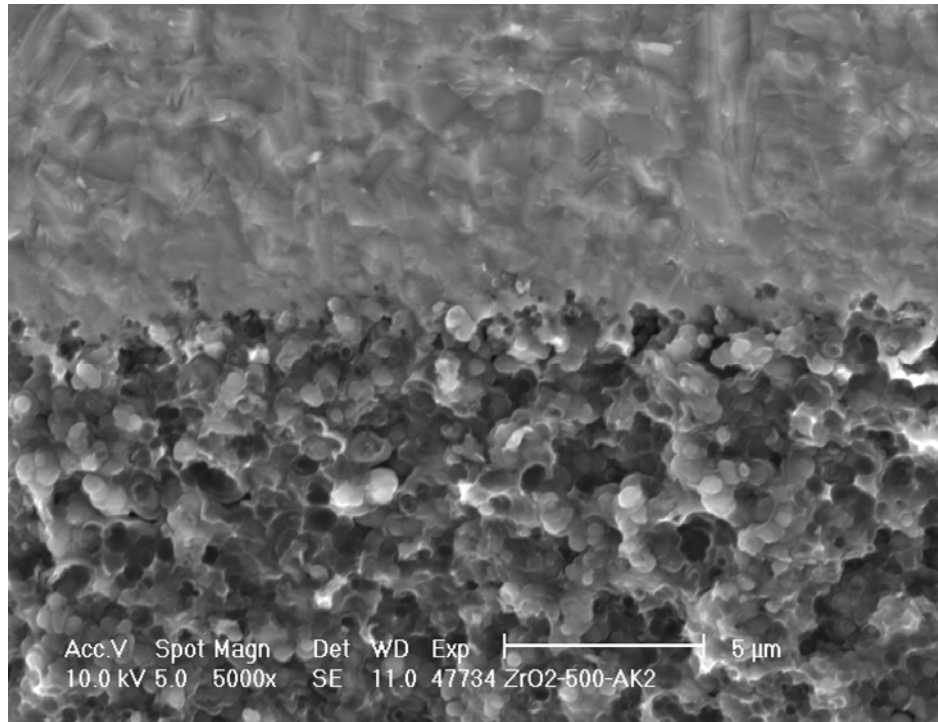
Figure 2-4: IPyC & SiC fracture surfaces (SEM, secondary electron).
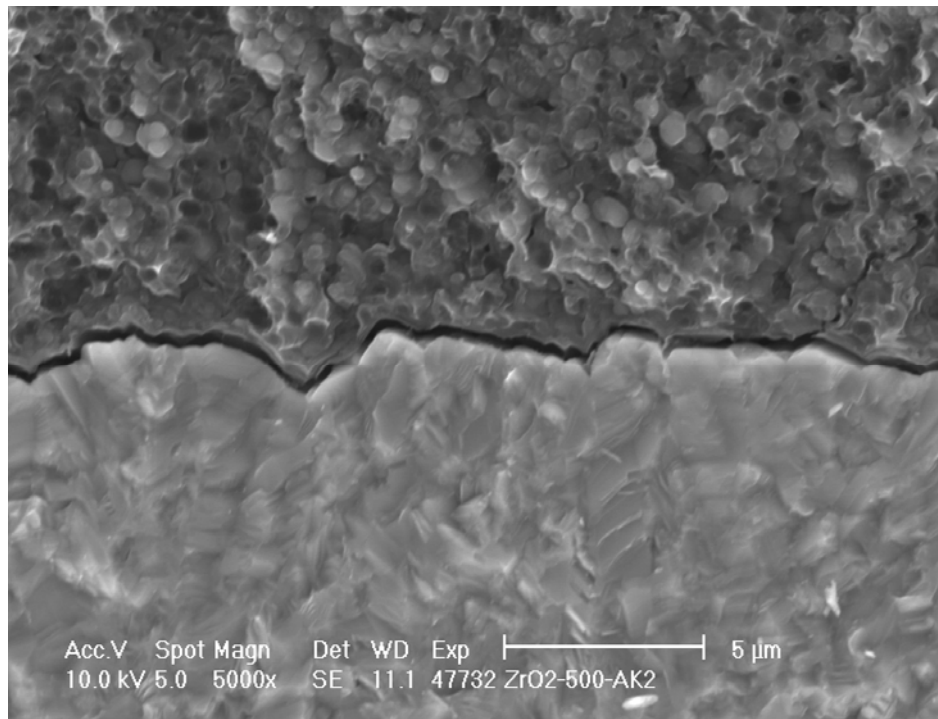
Figure 2-5: SiC & OPyC fracture surfaces (SEM, secondary electron)
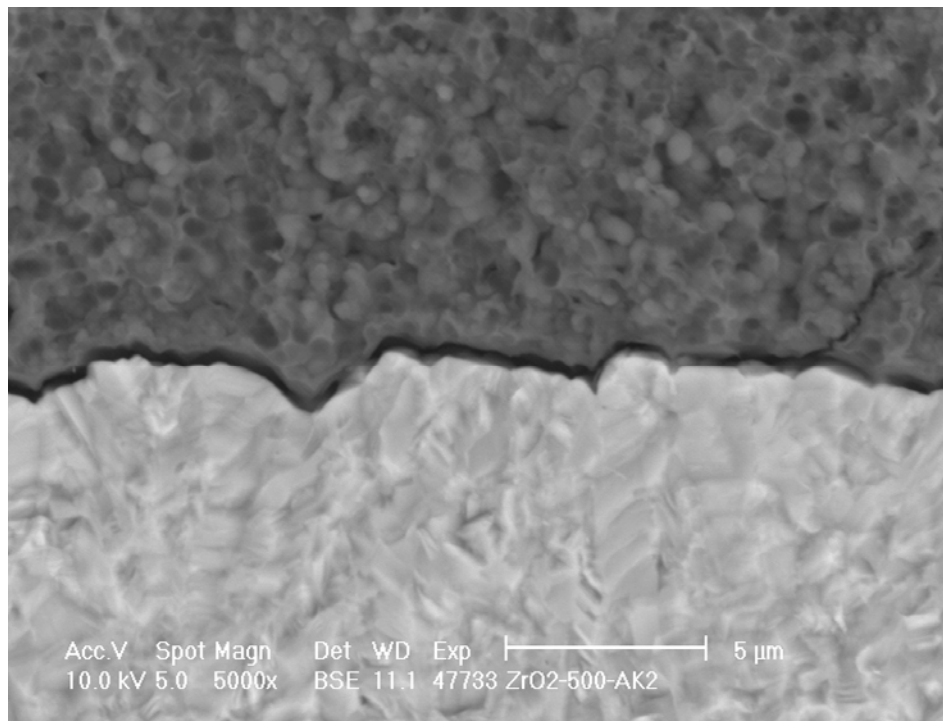
Figure 2-6: SiC & OPyC fracture surfaces (SEM, backscatter electron mode).
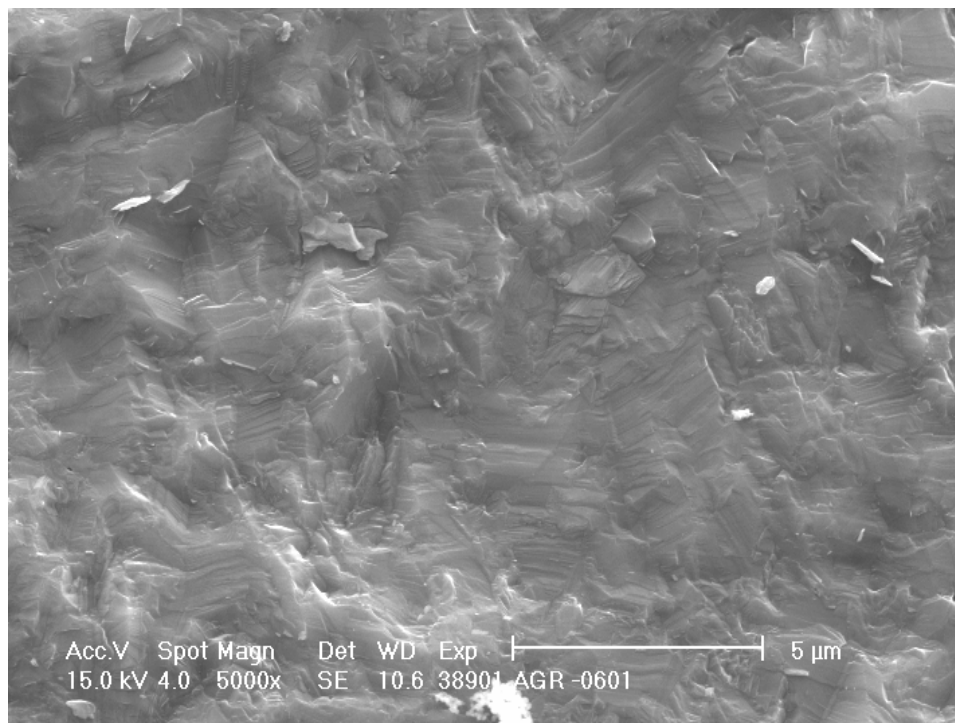
Figure 2-7: SiC fracture surface of German reference fuel (SEM, secondary electron)

3   Measurement of Size and Shape Using Shadowgraphy

J.D. Hunn, A.K. Kercher, and J.R. Price

3.1   Size and shape of kernels

Size and shape measurements of the YSZ kernels by shadowgraphy has not been performed. Approximate measurements of kernel size were performed on cross sectioned samples. The data is reported in section 4.1.

3.2   Size and shape of coated particles

Shadow images were obtained for a random orientation of 1368 coated particles sampled from ZrO2-500-AK2. Image analysis software was used to find the center of each kernel and identify 360 points around the perimeter. The uncertainty for this measurement was ±1.1 μm. This data was then compiled to report aspect ratios (maximum radius/minimum radius), mean radius, standard deviation in radius, maximum radius, and minimum radius for each particle measured. The summary data from each particle in the sample was then compiled to obtain the average, standard deviation, maximum, and minimum of the individual particle quantities (aspect ratios, mean radius, standard deviation in radius, maximum radius, and minimum radius). Figure 3-1 contains the compiled data and shows the distributions of the radius aspect ratio and mean particle radius. The histogram labels correspond to the maximum value in that bin (top of bin). The same data was also computed in terms of diameter by measuring the distance between perimeter points that were separated by 180°. These values are summarized in Figure 3-2. The average and standard deviation of the mean diameter were exactly twice the values obtained for the mean radius. Thus, the statistical measurement for the size distribution was equivalent for the two methods. The radius aspect ratio is more sensitive to the faceting and non-symmetrical features than the diameter aspect ratio; as is observed, the average radius aspect ratio would be expected to be higher for typical TRISO particles. A higher average and standard deviation was observed for the radius aspect ratio than for the diameter aspect ratio.

The measured particles had an average mean radius of 454 μm with a standard deviation in the distribution of 9 μm. Based on variable sampling statistics using a two-sided student's t distribution (t=1.96), the average mean radius of the ZrO2-500-AK2 particles was 453-455 μm with 95% confidence. The largest particle measured had a mean radius of 494 μm. The smallest particle had a mean radius of 421 μm.

	Radius Aspect Ratio	Mean Radius	St. Dev. In Radius	Minimum Radius	Maximum Radius
Average	1.072	454	8	438	469
Standard Deviation	0.021	9	2	10	10
Minimum	1.027	421	3	406	434
Maximum	1.331	494	35	469	561

Aspect Ratio (R)	Frequency
1	0
1.01	0
1.02	0
1.03	1
1.04	35
1.05	124
1.06	263
1.07	279
1.08	250
1.09	193
1.1	110
1.11	57
1.12	21
1.13	20
1.14	4
1.15	4
1.16	1
1.17	2
1.18	2
1.19	1
More	1
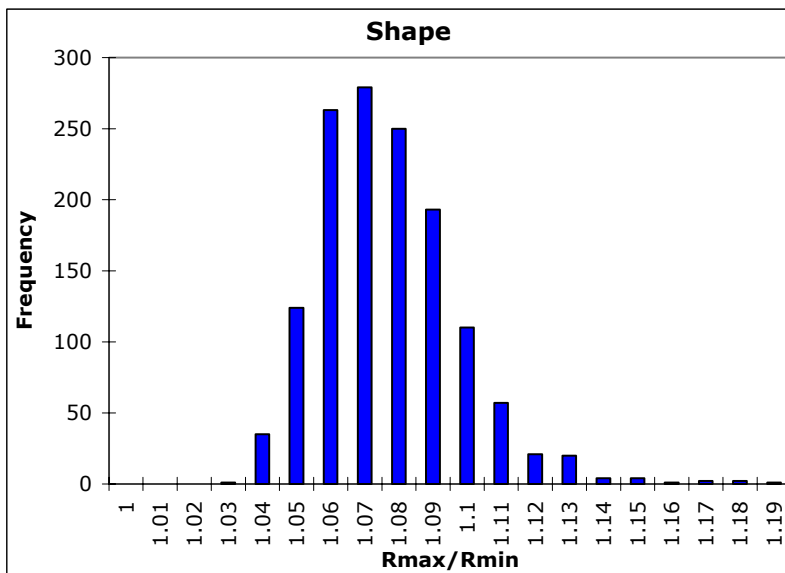
Mean Radius	Frequency
425	1
430	4
435	8
440	50
445	124
450	228
455	332
460	301
465	164
470	104
475	32
480	17
485	1
490	1
495	1
More	0
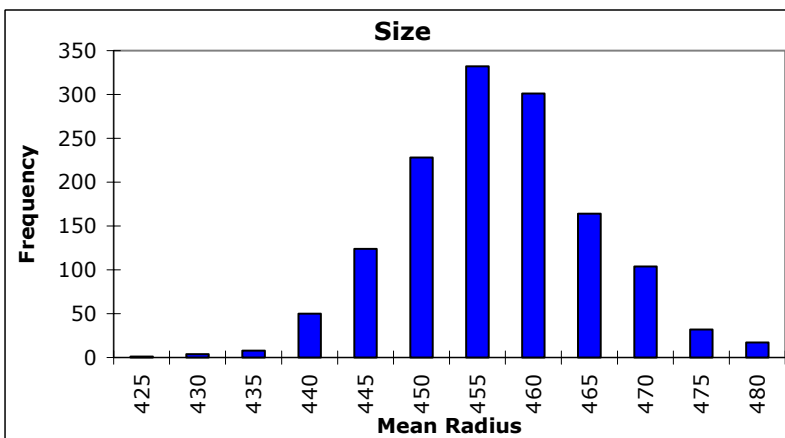
Figure 3-1: Size and shape summary for 1368 coated particles. Measurements are distance from best circle fit center to edge in μm.

	Diameter Aspect Ratio	Mean Diameter	St. Dev. In Diameter	Minimum Diameter	Maximum Diameter
Average	1.045	909	12	887	928
Standard Deviation	0.016	17	4	18	20
Minimum	1.011	843	3	823	856
Maximum	1.227	985	63	951	1089

Aspect Ratio (D)	Frequency
1	0
1.005	0
1.01	0
1.015	5
1.02	23
1.025	54
1.03	119
1.035	154
1.04	186
1.045	195
1.05	182
1.055	125
1.06	112
1.065	76
1.07	51
1.075	30
1.08	21
1.085	15
1.09	9
1.095	4
1.1	1
More	6
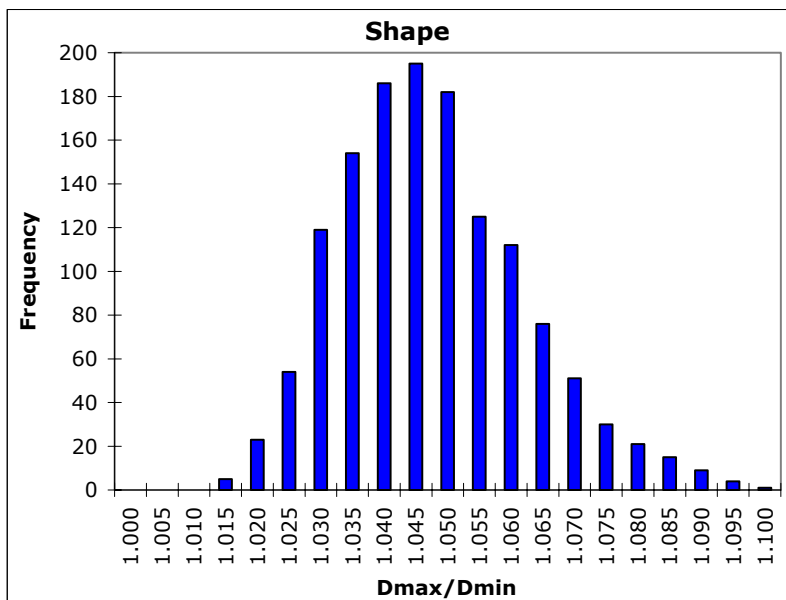
Mean Diameter	Frequency
850	1
860	3
870	9
880	53
890	118
900	230
910	329
920	299
930	168
940	109
950	27
960	18
970	2
980	1
990	1
More	0
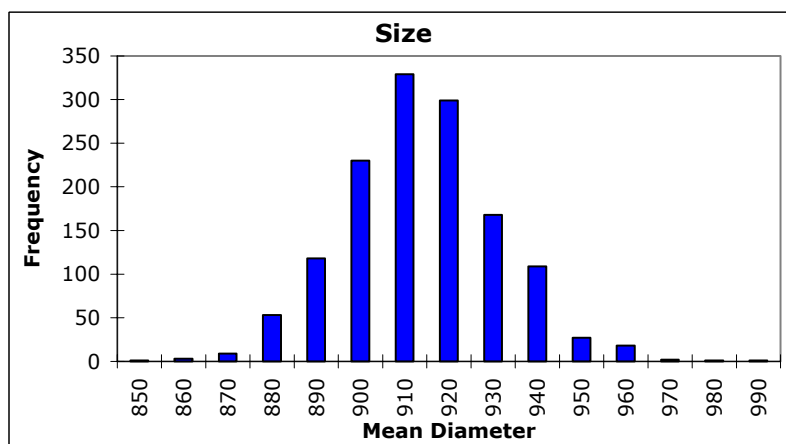
Figure 3-2: Size and shape summary for 1368 coated particles. Measurements are in μm from edge to edge through best circle fit center.

10

A diameter aspect ratio is the conventional method for describing the shape of TRISO fuel particles. The average diameter aspect ratio was 1.045 (Figure 3-2). In the lot, the 99th percentile for the diameter aspect ratio was between 1.08 and 1.11 to 95% confidence. The computer automated microscopy technique used by ORNL also readily provides the data to compute radius aspect ratios. The average radius aspect ratio (R_{max}/R_{min}) was 1.072 (Figure 3-1). In the lot, the 99th percentile for the radius aspect ratio was between 1.12 and 1.16 to 95% confidence. Faceting is the major source of asphericity in the ZrO2-500-AK2 particles (as is commonly seen in other TRISO particles). Because facets are defects that are radially asymmetric, particle faceting provides markedly different values for diameter aspect ratio and radius aspect ratio.
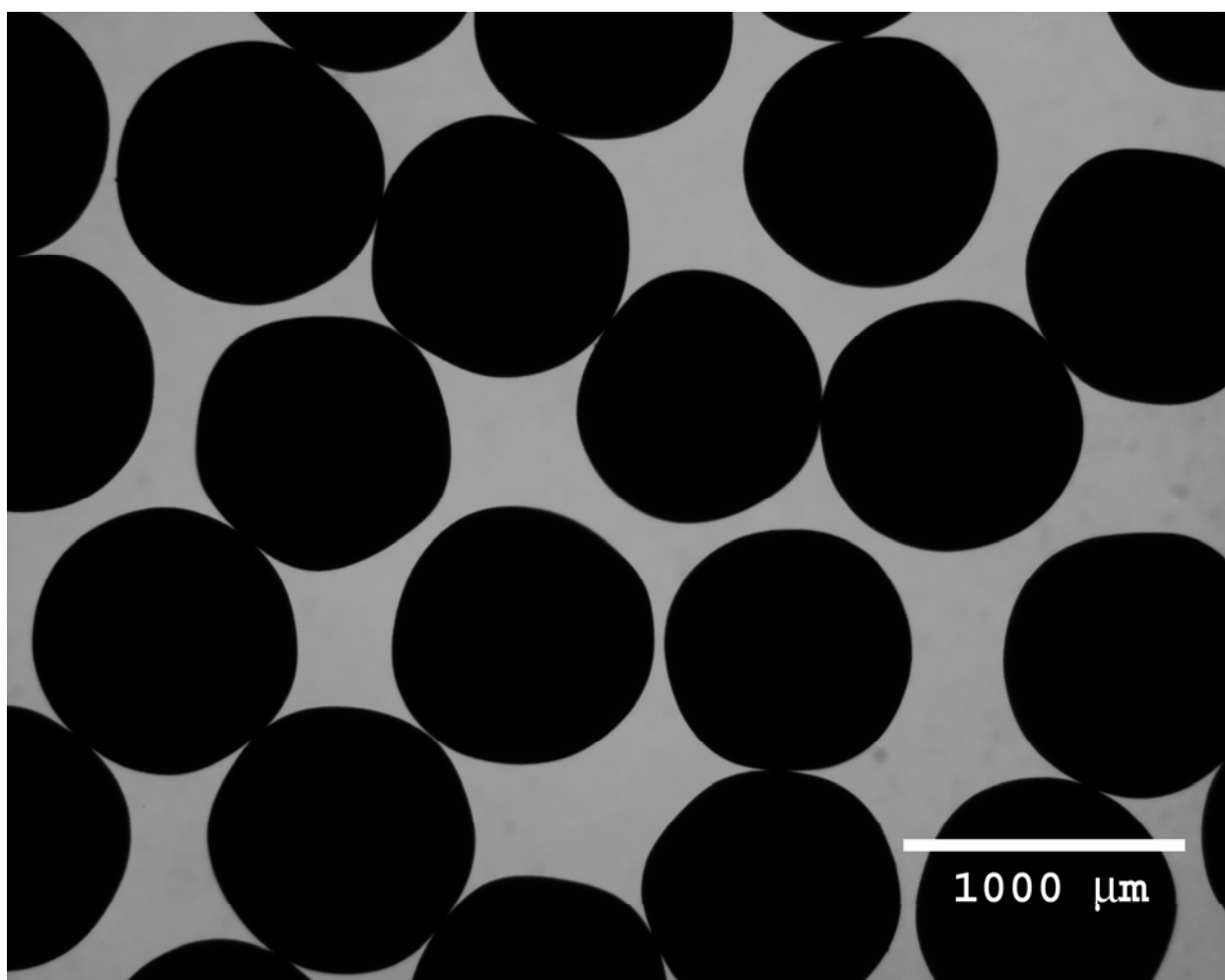
Figure 3-3: ZrO2-500-AK2 TRISO surrogate particles.

	Radius Cmax	Cmax
Average	1.73	0.0037
Standard Deviation	0.25	0.0005
Minimum	1.30	0.0027
Maximum	3.14	0.0063

Radius Cmax	Frequency
1.3	1
1.4	44
1.5	154
1.6	270
1.7	259
1.8	214
1.9	160
2	107
2.1	59
2.2	48
2.3	12
2.4	12
2.5	12
2.6	4
2.7	3
2.8	2
2.9	1
3	3
3.1	1
3.2	2
More	0
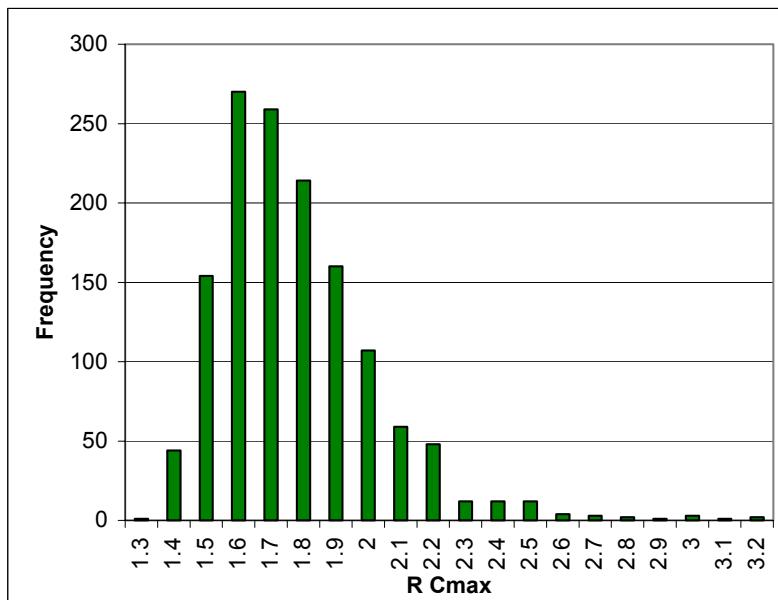
Figure 3-4: An alternate metric for shape, RC_{max}, has been developed at ORNL.

In TRISO fuel particles, the probability of layer fracture depends on the layer shape and consequently the particle shape. Computer models have correlated the probability of layer fracture to the sharpness of features on TRISO particles. Aspect ratios describe general particle shape and have not been strongly correlated to particle fracture mechanisms. At ORNL, a new metric has been developed that quantifies the sharpest observed feature on each individual particle and that has been correlated to layer fracture by membrane theory approximations. The new metric proposed by ORNL researchers is the product of the curvature and the radius at the point of maximum curvature (RC_{max}). Curvature is computed in the FFT (fast Fourier transform) domain using ten harmonics based on the equation:

$$C = \frac{x'y'' - y'x''}{(x'^2 + y'^2)^{3/2}}$$

where x and y are the x and y coordinates of the point on the boundary (based on a FFT fit). The sharpest feature observed for a particle occurs at the point of maximum curvature, and the curvature (C_{max} given in μm^{-1}) is multiplied by the local radius to make a unitless metric that is independent of particle size. While this recently devised metric is not currently used to qualify TRISO fuel, this information has been calculated for TRISO materials in the AGR program because of its potential future value in modeling fuel performance. Figure 3-4 contains a histogram of RC_{max} for ZrO2-500-AK2 and associated data. The average value for RC_{max} was 1.73. In the lot, the 99th percentile for RC_{max} was between 2.46 and 2.99 to 95% confidence.

4   Measurement of Coating Thicknesses

J.D. Hunn, A.K. Kercher, and J.R. Price

Coating thicknesses were measured on 127 particles by mounting particles in a clear epoxy and grinding and polishing the particles to close to, but not beyond, the midpoint. The polished cross sections were imaged in bright field reflected mode with a computer-automated optical microscope and the images were computer analyzed to extract the thickness information for each layer. The deviation of the measured layer thickness from the actual layer thickness due to the polished cross section not being exactly at a midplane was corrected by measuring the outer diameter of the particle and applying a geometric correction. The outer diameter was measured by backlighting the clear epoxy mount to obtain a shadow image of the particle in addition to the bright field reflected image.

4.1   Kernel diameter

Kernel diameter and radius aspect ratio was determined by cross-section analysis. This is not the preferred method for determination of kernel size and shape, but unfortunately the original kernels were not imaged and no sample of those surrogate kernels is currently available. There is potentially a much larger uncertainty in determining size and shape of the kernels by cross-section when compared to using shadowgraphic methods. The deviation from midplane was corrected, as noted above, however, the associated error in this correction was greater than it was for the coatings due to the fact that the kernel edge was closer to the geometric center of the particle and to the fact that the kernels may have been off center in some cases.

Figure 4-1 shows the data summary for the kernel radius. The histogram labels correspond to the maximum value in that bin (top of bin). The average mean radius was 265 μm with a standard deviation of 9 μm. The average R_{max}/R_{min} was 1.02. The aspect ratio was adjusted by a systematic offset error associated with extracting a ratio of a maximum value over a minimum value (which is based on pixel size and average kernel radius, as discussed in depth in ORNL/CF-04/07). Based on variable sampling statistics using a two-sided student's t distribution (t=1.98), the average mean diameter of the YSZ kernels was 528-534 μm with 95% confidence. The kernel manufacturer (Nikkato Corporation) supplied an inspection sheet for the kernel lot. According to the manufacturer, the average kernel diameter was 526.1 μm with a standard deviation in the sample of 17.1 μm for a sample size of 100 kernels. The reasonably close agreement with manufacturer data suggested that the measurement bias or measurement uncertainty caused by extracting kernel size from cross-sections was probably small.

	Rmax/Rmin	Mean Radius	Stnd. Dev. In Radius	Minimum Radius	Maximum Radius
Average	1.02	265	1.6	262	269
Standard Deviation	0.008	9	0.5	9	10
Maximum	1.06	287	4	284	291
Minimum	1.01	242	0.7	238	245

Rmax/Rmin	Frequency
1	0
1.01	3
1.02	59
1.03	48
1.04	16
1.05	0
1.06	1
More	0

Mean Radius	Frequency
245	2
250	4
255	10
260	18
265	27
270	24
275	25
280	8
285	6
290	3
More	0
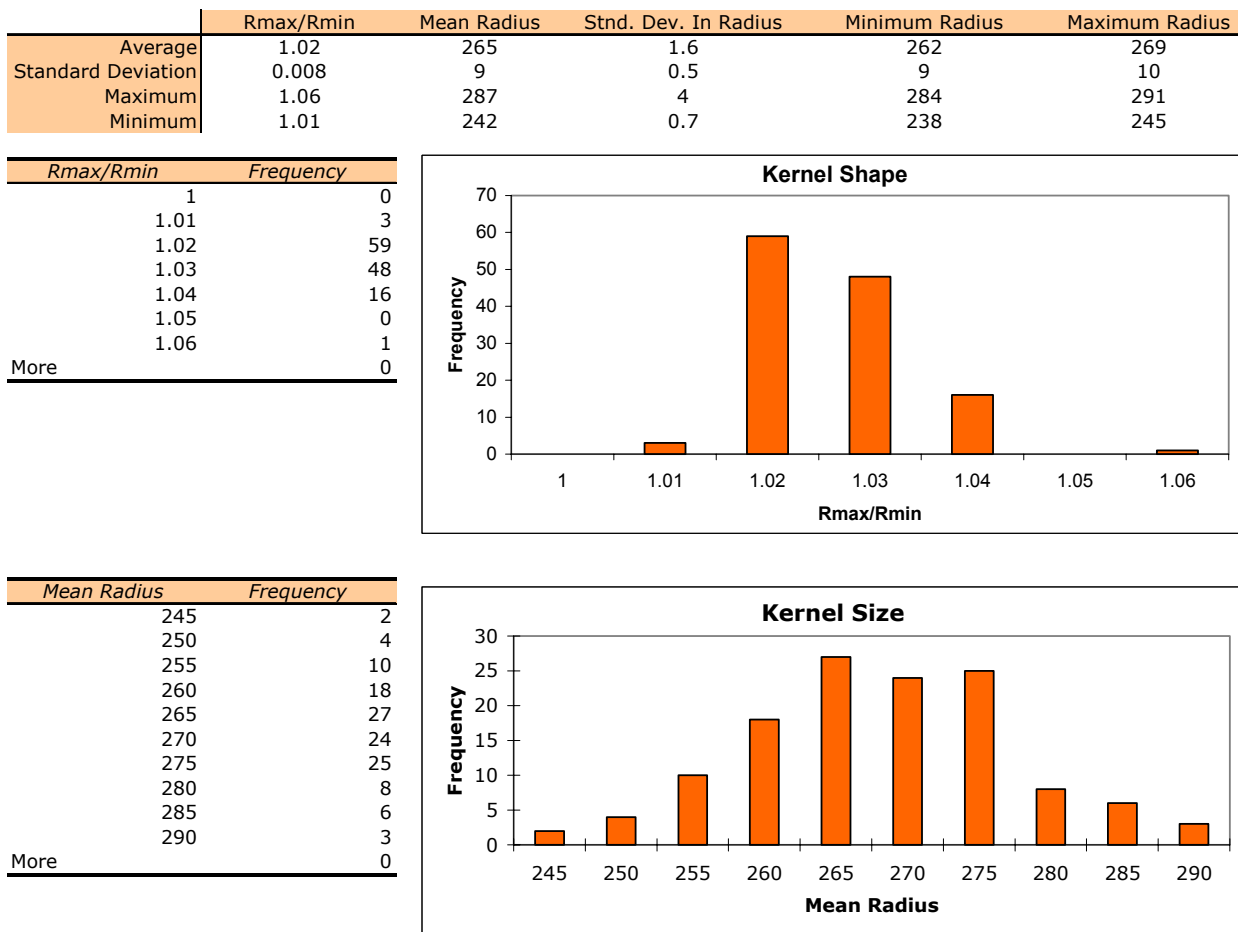
Figure 4-1: Data summary for kernel radius from cross section measurement. Radii are in μm.

4.2 Buffer thickness

Figure 4-2 shows the data summary for the measurements made on the buffer. The average mean buffer thickness was 85 μm with a standard deviation in the distribution of 7 μm. Based on variable sampling statistics using a two-sided student's t distribution (t=1.98), the average mean thickness of the buffer in this lot of particles was 84-86 μm with 95% confidence. The thickest buffer layer was 105 μm (average). The thinnest buffer layer was 71 μm (average).

	Mean Thickness	Stnd. Dev. In Thickness	Maximum Thickness	Minimum Thickness
Average	85	4	94	76
Standard Deviation	7	1.1	8	6
Maximum	105	9	119	95
Minimum	71	2	79	63

Mean Thickness	Frequency
75	6
80	26
85	35
90	36
95	14
100	5
105	4
More	0

Figure 4-2: Data summary for buffer thickness. Thicknesses are in μm.

4.3 IPyC thickness

Figure 4-3 shows the data summary for the measurements made on the IPyC. The average mean IPyC thickness was 41 μm with a standard deviation in the distribution of 2 μm. Based on variable sampling statistics using a two-sided student's t distribution (t=1.98), the average mean IPyC thickness of the ZrO2-500-AK2 particles was 40-42 μm with 95% confidence. The thickest IPyC layer was 50 μm (average). The thinnest IPyC layer was 36 μm (average).

	Mean Thickness	Stnd. Dev. In Thickness	Maximum Thickness	Minimum Thickness
Average	41	3	49	36
Standard Deviation	2	0.8	4	3
Maximum	50	7	59	45
Minimum	36	1.0	41	30

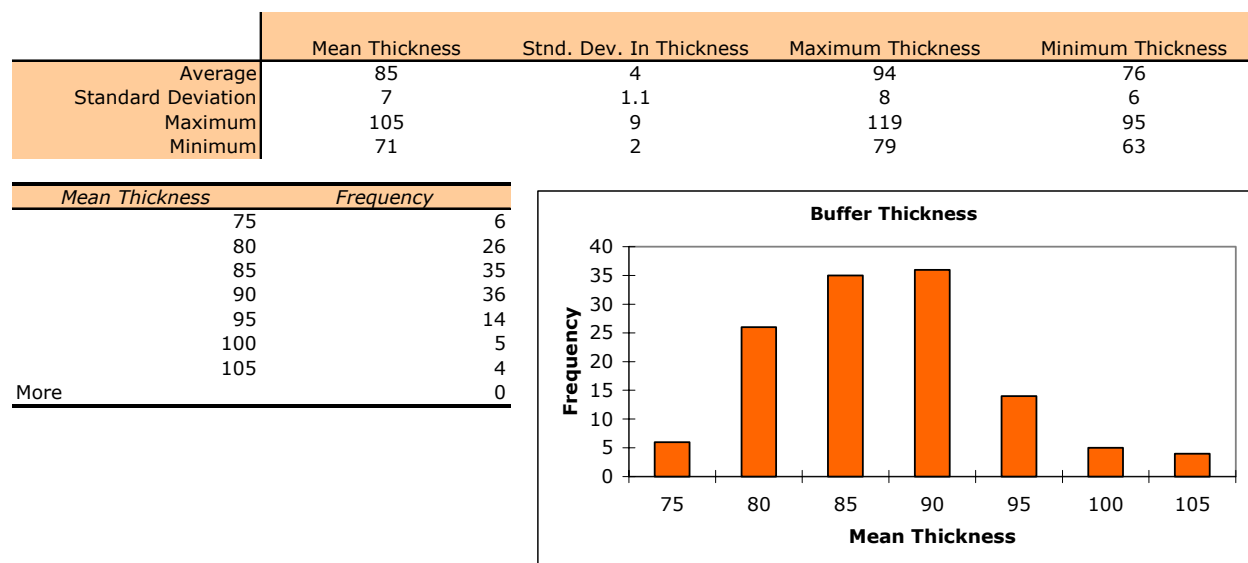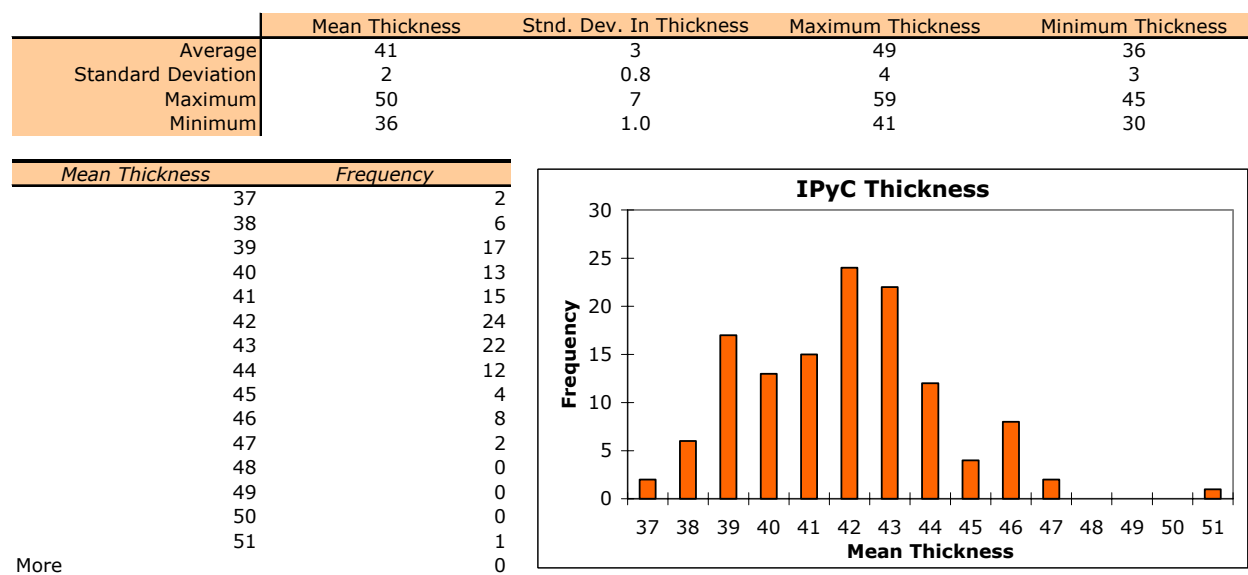| Mean Thickness	Frequency
37	2
38	6
39	17
40	13
41	15
42	24
43	22
44	12
45	4
46	8
47	2
48	0
49	0
50	0
51	1
More	0

Figure 4-3: Data summary for IPyC thickness. Thicknesses are in μm.

4.4   SiC thickness

Figure 4-4 shows the data summary for the measurements made on the SiC. The average mean SiC thickness was 31 μm with a standard deviation in the distribution of 1.0 μm. Based on variable sampling statistics using a two-sided student's t distribution (t=1.98), the average mean SiC thickness of the ZrO2-500-AK2 particles was 30-32 μm with 95% confidence. The thickest SiC layer was 33 μm (average). The thinnest SiC layer was 27 μm (average).

	Mean Thickness	Stnd. Dev. In Thickness	Maximum Thickness	Minimum Thickness
Average	31	1.1	33	28
Standard Deviation	1.0	0.2	1.2	1.1
Maximum	33	1.8	36	31
Minimum	27	0.6	30	24

Mean Thickness	Frequency
28	2
29	5
30	19
31	59
32	32
33	9
34	1
More	0

Figure 4-4: Data summary for SiC thickness. Thicknesses are in μm.

4.5   OPyC thickness

Figure 4-5 shows the data summary for the measurements made on the OPyC. The average mean OPyC thickness was 36 μm with a standard deviation in the distribution of 1.6 μm. Based on variable sampling statistics using a two-sided student's t distribution (t=1.98), the average mean OPyC thickness of the ZrO2-500-AK2 particles was 35-37 μm with 95% confidence. The thickest OPyC layer was 40 μm (average). The thinnest OPyC layer was 31 μm (average).
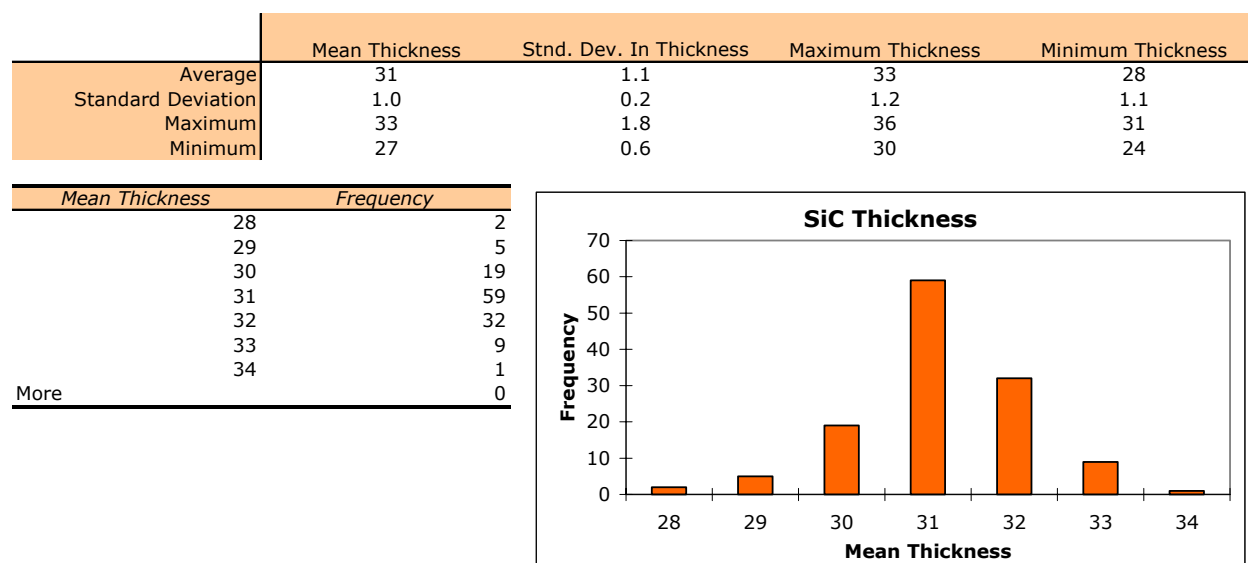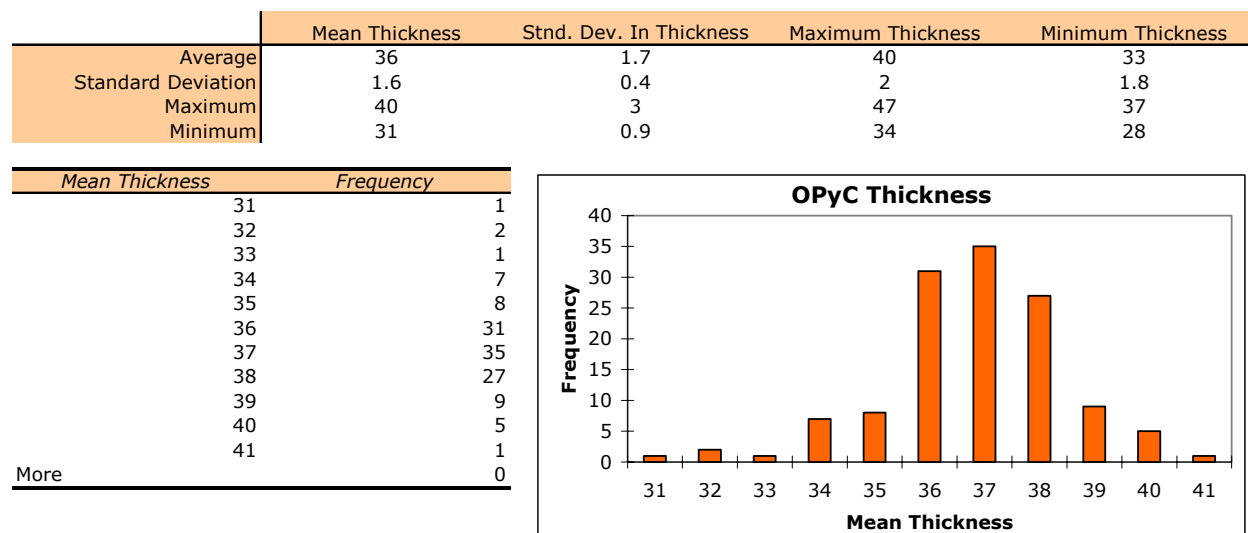
	Mean Thickness	Stnd. Dev. In Thickness	Maximum Thickness	Minimum Thickness
Average	36	1.7	40	33
Standard Deviation	1.6	0.4	2	1.8
Maximum	40	3	47	37
Minimum	31	0.9	34	28

Mean Thickness	Frequency
31	1
32	2
33	1
34	7
35	8
36	31
37	35
38	27
39	9
40	5
41	1
More	0

OPyC Thickness

Figure 4-5: Data summary for OPyC thickness. Thicknesses are in μm.

4.6   Total particle radius

The mean kernel radius and mean layer thickness data were summed for each particle as a comparison check against the data obtained from the whole particle shadowgraphy measurements made in section 3.2. The average mean radius obtained by summing the data from the cross section measurements was 459 μm with a standard deviation in the distribution of 8 μm (Figure 4-6). This agreed fairly well with the data obtained by shadow imaging the whole particles summarized in Figure 3-1 (454 ± 9 μm), especially considering the difficulties in measurement associated with the very odd shapes of the particles. The average radius aspect ratio (1.069) was nearly the same as measured by shadowgraphy (1.072).

	Rmax/Rmin	Mean Radius
Average	1.07	459
Standard Deviation	0.02	8
Maximum	1.15	487
Minimum	1.03	441

Rmax/Rmin	Frequency
1.04	7
1.05	6
1.06	33
1.07	30
1.08	19
1.09	16
1.1	10
1.11	0
1.12	3
1.13	0
1.14	1
1.15	1
More	0
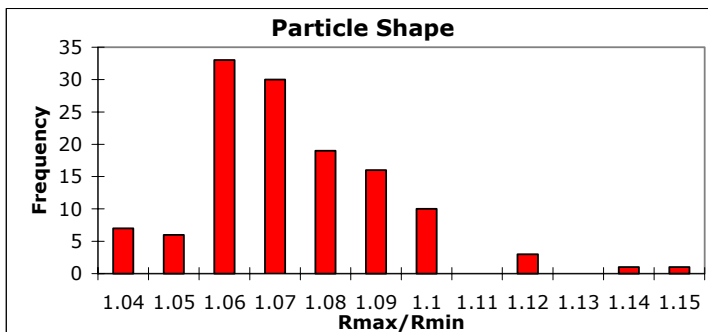
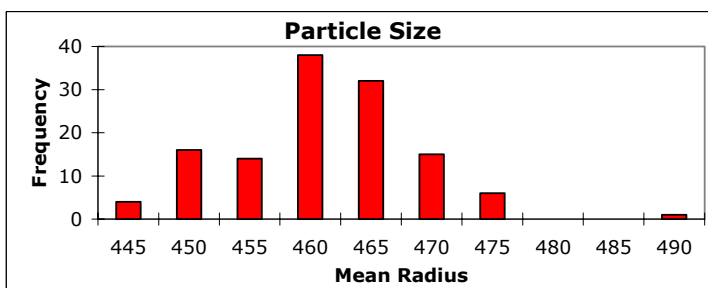| Mean Radius	Frequency
445	4
450	16
455	14
460	38
465	32
470	15
475	6
480	0
485	0
490	1
More	0

Figure 4-6: Data summary for total particle radius and radius aspect ratio from cross-section analysis. Total particle radius calculated from sum of kernel radius and layer thicknesses. Radii are in μm.

5   Density Measurement

D.L. Barker and J.D. Hunn

5.1   SiC density

The particle coatings were broken away from the kernel by placing several particles at a time into a stainless steel cylindrical dye and applying light pressure with a stainless steel cylindrical ram. Pieces of IPyC/SiC fragments were removed and heated in air at 750°C for 90 min to remove the carbon layers. The separated SiC fragments were placed in a liquid gradient density column spanning a range of 3.15-3.21 g/cc. The column was created using an appropriate combination of methylene iodide and bromoform in such a way as to create a linear density gradient. Six calibration floats were used to generate a density versus position linear fit for the column and the density of the SiC fragments was calculated after measuring their equilibrium position in the column. Figure 5-1 shows the column calibration and measured values for 14 SiC fragments. The average density measured by this method was 3.2048 g/cc (standard deviation of the sample = 0.0015; standard error of the mean = 0.0004). The 95% confidence interval for the average SiC density by this method was 3.204-3.206 g/cc. The density measured by this technique is expected to have a value between the envelope density and the skeletal density, depending on the porosity of the material and the extent to which the liquid penetrates the open pores. The SiC had very little porosity, so there should be little difference between the envelope density and the skeletal density.

ZRO2-500-AK2
SiC

Calibrated Floats

Density	Top of Float	Bottom of Float	Float Position
3.150	73.64	97.20	85.42
3.170	183.84	207.21	195.53
3.190	313.81	335.94	324.88
3.200	384.95	404.36	394.66
3.210	457.91	481.46	469.69

Linear Fit

slope	intercept
1.56E-04	3.14E+00

Particle Number	Particle Position	Calculated Density
1	415.54	3.203
2	418.55	3.203
3	420.94	3.204
4	425.75	3.205
5	428.04	3.205
6	430.99	3.205
7	434.06	3.206
8	436.07	3.206
9	438.02	3.206
10	440.62	3.207
11	449.54	3.208
12	438.26	3.206
13	432.43	3.206
14	441.13	3.207

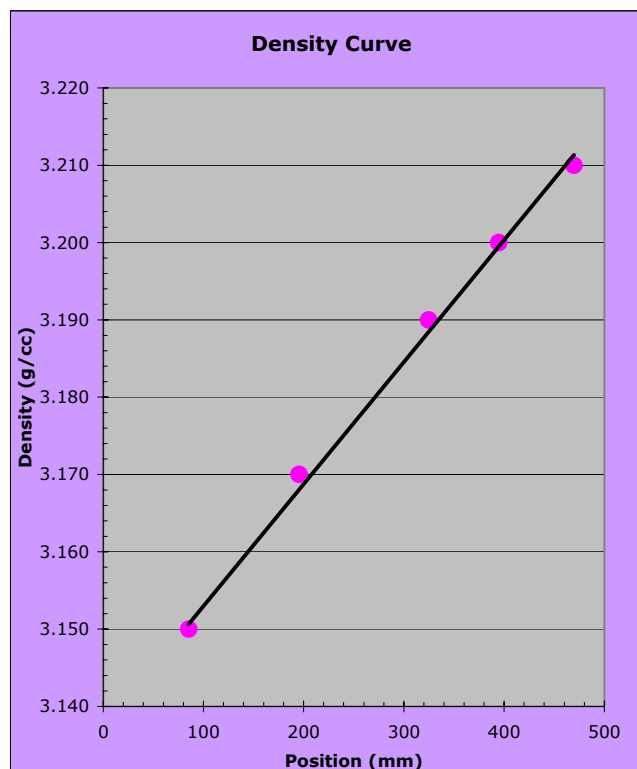| Average	3.205
Standard Deviation	0.001

Density Curve

Figure 5-1: Density column data report for SiC. Densities are in g/cc.

5.2   OPyC density

Coatings were broken off of the particles as described in section 5.1. Pieces of free OPyC fragments were removed. The separated OPyC fragments were placed in a liquid gradient density column spanning a range of 1.7-2.1 g/cc. The column was created using an appropriate combination of ethylene bromide and tetrachloroethylene in such a way as to create a linear density gradient. Four calibration floats were used to generate a density versus position linear fit for the column that spanned the range of the unknown. The density of the OPyC fragments was calculated after measuring their equilibrium position in the column. Figure 5-2 shows the column calibration and measured values for the OPyC fragments. The average density measured by this method was 2.0119 g/cc (standard deviation of the sample = 0.0018; standard error of the mean = 0.0005). The 95% confidence interval for the average OPyC density by this method was 2.011-2.013 g/cc.
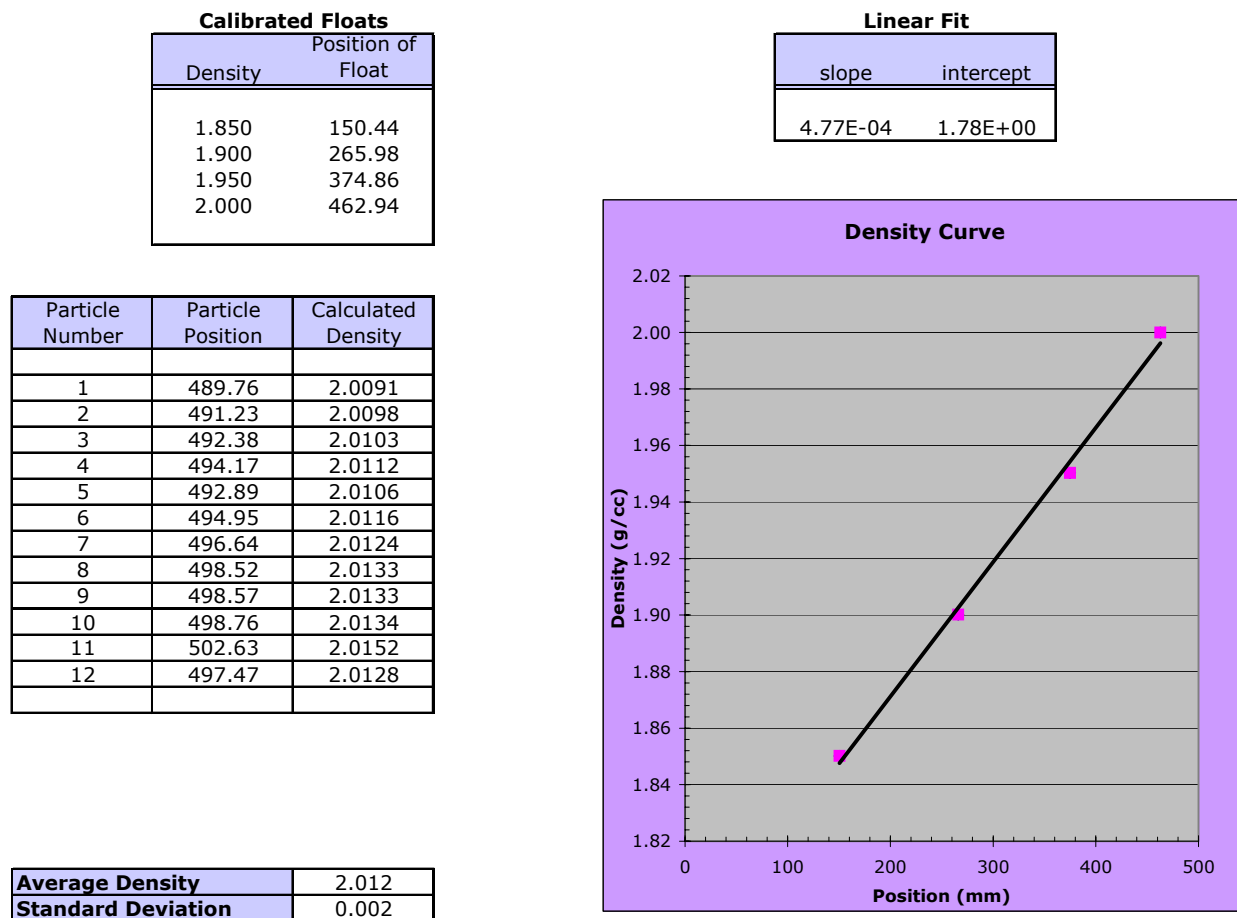
20

Calibrated Floats

| | Position of |
Density	Float
1.850	150.44
1.900	265.98
1.950	374.86
2.000	462.94

Linear Fit

slope	intercept
4.77E-04	1.78E+00

Particle Number	Particle Position	Calculated Density
1	489.76	2.0091
2	491.23	2.0098
3	492.38	2.0103
4	494.17	2.0112
5	492.89	2.0106
6	494.95	2.0116
7	496.64	2.0124
8	498.52	2.0133
9	498.57	2.0133
10	498.76	2.0134
11	502.63	2.0152
12	497.47	2.0128

Average Density	2.012
Standard Deviation	0.002

Density Curve

Figure 5-2: Density column data report for OPyC. Densities are in g/cc.

The density measured by this technique is expected to have a value between the envelope density and the skeletal density, depending on the porosity of the material and the extent to which the liquid penetrates the open pores. OPyC does have significant porosity, so it is uncertain where the density based on density column data falls relative to the envelope and skeletal densities.

6   <u>Optical Anisotropy Measurements</u>

G. E. Jellison, Jr. and J. D. Hunn

Particles were mounted and polished to reveal the individual coatings and a series of optical anisotropy measurements were made using the two-modulator generalized ellipsometry microscope (2-MGEM). The 2-MGEM measured the average Mueller matrix in a 4 µm diameter spot which was scanned over the specimen surface in two dimensions with a 2 µm step size in each direction. With this data, various optical anisotropy parameters could be imaged with a 2x2 µm per pixel resolution. A data set containing 2-MGEM data for 182,000 spots was generated for each particle.

Images produced by the 2-MGEM were analyzed using a software tool developed for this project which allowed for individual pixels in the image to be selected and added to different lists. Using this tool, data was grouped together for the kernel (used for final data normalization), the IPyC layer and the OPyC layer. Data points can be selected using any of the optical parameter images. The diattenuation is often used. In some cases, such as when the diattenuation is near zero, it is more convenient to use the reflected intensity image in order to be able to identify the individual layers. Any one of the pictures can be displayed in the data sheet.

The diattenuation and the direction of the fast axis were measured. It was assumed that the diattenuation was the primary quantity, and it was set to be positive definite and was used to determine the direction of the fast axis. In the data sheet, the average and standard deviation (SD) of the data in each list was calculated. The average error (that is, the average of the error limits for each of the selected parameters measured at each point) was also calculated for the diattenuation. If there is a significant variation of the observed quantity around the layer, then the SD will be on the order of or greater than the average error, but if the quantity is uniform at all the selected points in the list, then the SD will be less than the average error.

In the PyC layers, the technique of characterizing crystalline anisotropy by measuring average optical anisotropy is based on the fact that the graphite structure possesses a high optical anisotropy. Sixteen separate particles were measured (Table 6-1). The IPyC layer had a significant diattenuation, N = 0.0145±0.0008. This corresponds to an optical anisotropy factor of 1.029±0.0017 [OAF = (1+N)/(1-N)]. The direction of the fast axis (which can range from -90° to +90°, corresponding to the average in-plane direction of the a-b plane) was roughly perpendicular to the growth direction. The net fast axis orientation was measured for each pixel. The standard deviation of the fast axis orientation for each particle was averaged to obtain a measure of graphene sheet alignment in the microstructure, which was called the average standard deviation of the fast axis orientation (ASD-FAO). The ASD-FAO was 8.5°±1.5°.

There was a smaller amount of optical anisotropy in the OPyC layer, again with the direction of the fast axis roughly perpendicular to the growth direction. Only six separate particles were analyzed (Table 6-2). The diattenuation was 0.0047±0.00099 (OAF = 1.009±0.002). This was 32% of the diattenuation measured for the IPyC layer. The ASD-FAO was 26.1°±5.3°, which indicated only a weak partial alignment of graphene sheets perpendicular to the growth direction.

It is important to note that the IPyC layer experienced the SiC deposition temperature and possible associated microstructural rearrangement, but the OPyC was not exposed to elevated temperature. As of the writing of this document, pyrocarbon microstructural change during SiC deposition has not yet been explored. Anisotropy results on OPyC may be less reliable than on IPyC due to rounding of the particle edge during cross-sectional polishing.

The measured anisotropies of the ZrO2-500-AK2 pyrocarbon layers were similar to those previously measured by the 2-MGEM for the German reference material. A total of 12 particles of German fuel were measured. The average of the average diattenuation for the IPyC layers was 0.0140±.0016 (OAF = 1.028±0.003). The average of the average diattenuation for the OPyC layers was 0.0080±0.0010 (OAF = 1.016±0.002).

Table 6-1: IPyC optical anisotropy data based on 2-MGEM measurements

Particle #	Average Diattenuation	Standard Deviation of Diattenuation	Average Error	Optical Anisotropy Factor	ASD-FAO
1	0.0153	0.0037	0.0036	1.031	8.5
2	0.0145	0.0031	0.0034	1.029	9.4
3	0.0150	0.0044	0.0040	1.030	13.1
4	0.0157	0.0044	0.0036	1.032	8.6
5	0.0138	0.0035	0.0035	1.028	7.6
6	0.0131	0.0033	0.0034	1.027	9.5
7	0.0153	0.0036	0.0027	1.031	9
8	0.0134	0.0032	0.0023	1.027	9.1
9	0.0154	0.0032	0.0022	1.031	6.1
10	0.0147	0.0037	0.0022	1.030	7.4
11	0.0144	0.0032	0.0040	1.029	8.4
12	0.0145	0.0032	0.0037	1.029	7.9
13	0.0148	0.0037	0.0034	1.030	7.9
14	0.0151	0.0032	0.0033	1.031	8.1
15	0.0131	0.0032	0.0034	1.027	7.4
16	0.0142	0.0031	0.0034	1.029	8.1
average	0.0145	0.0035	0.0033	1.029	8.5
st. dev.	0.0008	0.0004	0.0006	0.0017	1.5

Table 6-2: OPyC optical anisotropy data based on 2-MGEM measurements

Particle #	Average Diattenuation	Standard Deviation of Diattenuation	Average Error	Optical Anisotropy Factor	ASD-FAO
1	0.0049	0.0025	0.0041	1.010	27.7
2	0.0049	0.0017	0.0033	1.010	19.6
3	0.0028	0.0021	0.0039	1.006	35.1
4	0.0058	0.0025	0.0039	1.012	22.1
5	0.0046	0.0025	0.0038	1.009	26.3
6	0.0049	0.0026	0.0041	1.010	25.9
average	0.0047	0.0023	0.0039	1.009	26.1
st. dev.	0.00099	0.0003	0.0003	0.002	5.3

7   <u>SEM Analysis</u>

P.A. Menchhofer, J.D. Hunn, and I. Dunbar

7.1   SEM of coated particles

Each SEM analysis of ZrO2-500-AK2 was performed on an individual particle, so no statistical inferences about the microstructure can be made. Nonetheless, attempts were made to image "representative" particles so that SEM analysis should describe a typical ZrO2-500-AK2 particle. Figure 7-1 shows a typical particle cross-section with a bright kernel surrounded by a porous buffer surrounded by a dark gray IPyC layer, a bright SiC layer, and a dark gray OPyC layer.

No cracking or sudden microstructural transition was observed at the buffer/IPyC interface (Figure 7-2). The buffer layer had a substantial amount of porosity and perhaps slight porosity banding (Figure 7-3). The IPyC layer had significant porosity that was relatively randomly positioned; no porosity bands were observed in the IPyC layer (Figure 7-4). IPyC porosity bands have been previously observed in German TRISO fuel and historic U.S. TRISO experimental fuel. No consensus in the nuclear fuel community exists on the effect (if any) of IPyC porosity bands on fuel performance. It is hypothesized that a layered structure with bands of high porosity may result in a layer that is less permeable than one that has the same average envelope density but is more uniform throughout the thickness. The heterogeneous microstructure of the IPyC layer was studied using backscatter electron imaging (Figure 7-5). The flakes of carbon (dark gray) were formed by gas phase nucleation and later deposited onto the growing IPyC layer; the surrounding carbon material (light gray) grew on top of the carbon flakes before deposition or on top of the growing IPyC layer.

The interface between the IPyC and the SiC is shown in Figure 7-6. Extensive interfacial stitching without gaps was observed. The IPyC layer exhibited no significant increase in porosity at the IPyC/SiC interface. This interfacial structure has the potential to provide a strong bond between the IPyC and SiC layers under irradiation conditions.

The SiC layer had a fine grain structure with little porosity (Figure 7-7). The grains were predominantly asymmetric in shape, but a strong columnar microstructure was not observed. Figure 7-7 also enabled a side by side comparison of the IPyC/SiC and OPyC/SiC interfaces. The IPyC/SiC interface (right boundary of SiC layer) was shown to have extensive interfacial stitching, while the OPyC/SiC interface (left boundary of SiC layer) was shown to have no discernable interfacial stitching. A high magnification view of the OPyC/SiC interface is shown in Figure 7-8. Cracking can be observed along the OPyC/SiC interface (Figure 7-8). The OPyC layer had a similar porosity structure to the IPyC layer (Figure 7-9).
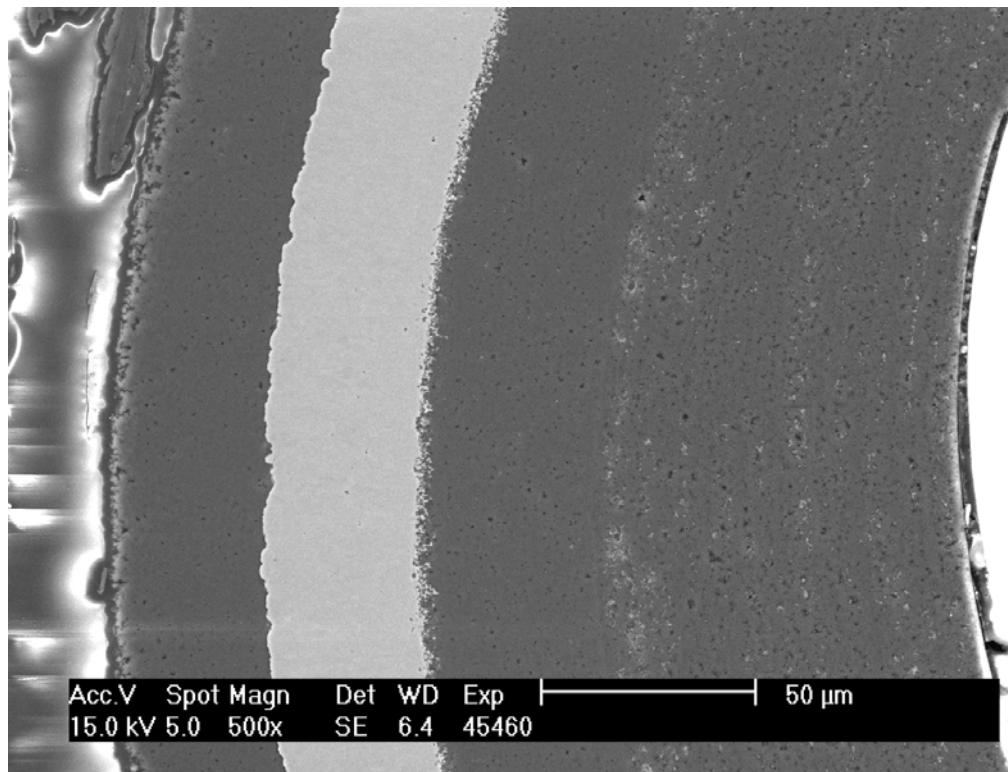
Figure 7-1: Typical coating layers for ZrO2-500-AK2 (secondary electron image).
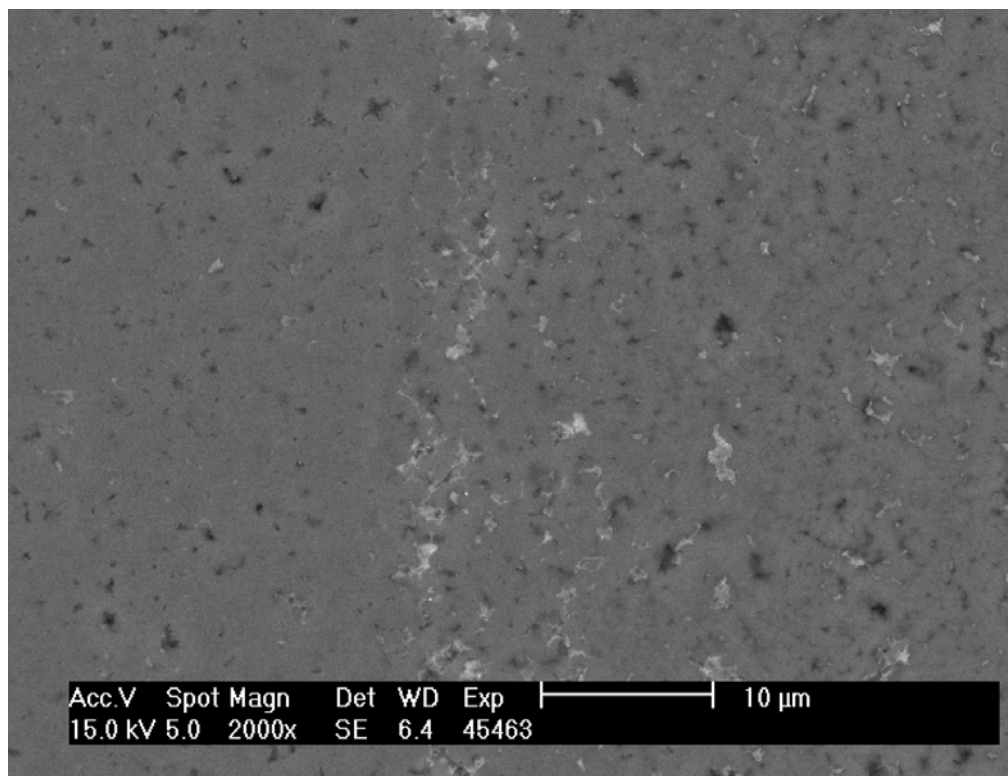

Figure 7-2: Buffer/IPyC interface in ZrO2-500-AK2 (secondary electron image).
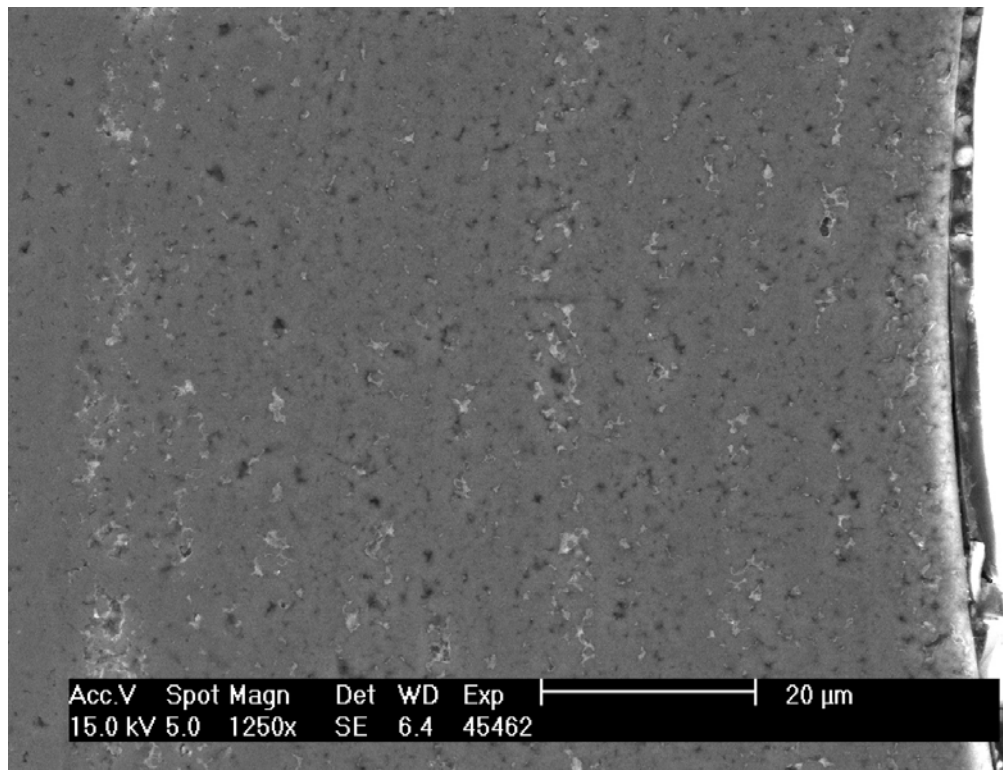
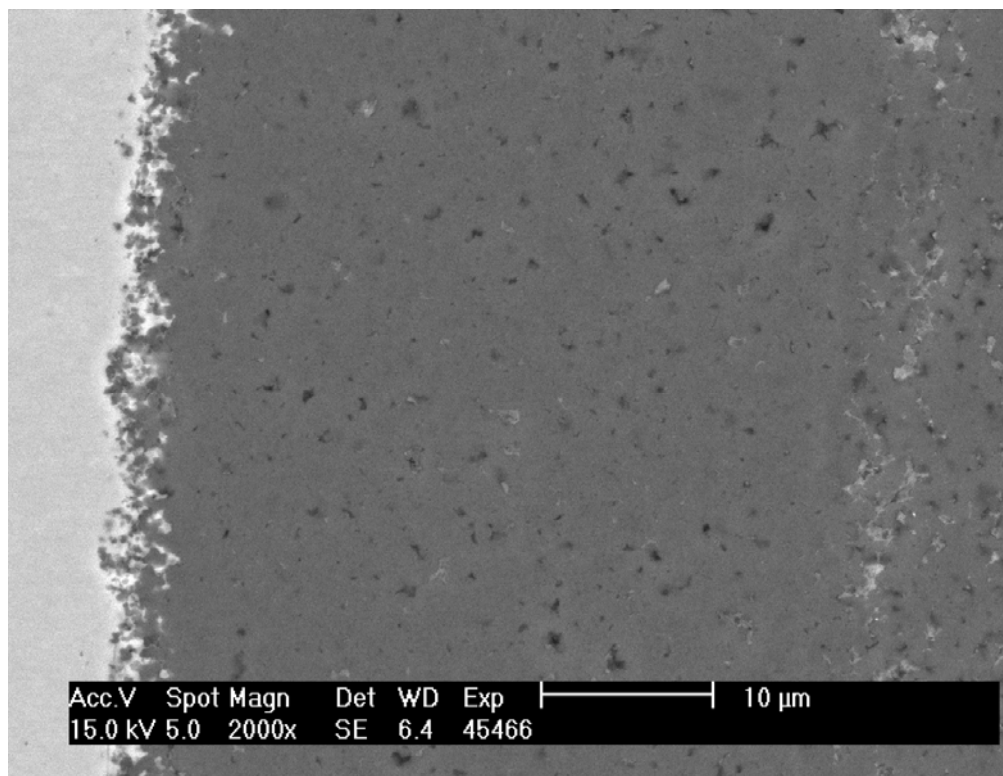**Figure 7-3:** Buffer layer of ZrO2-500-AK2 (secondary electron image).

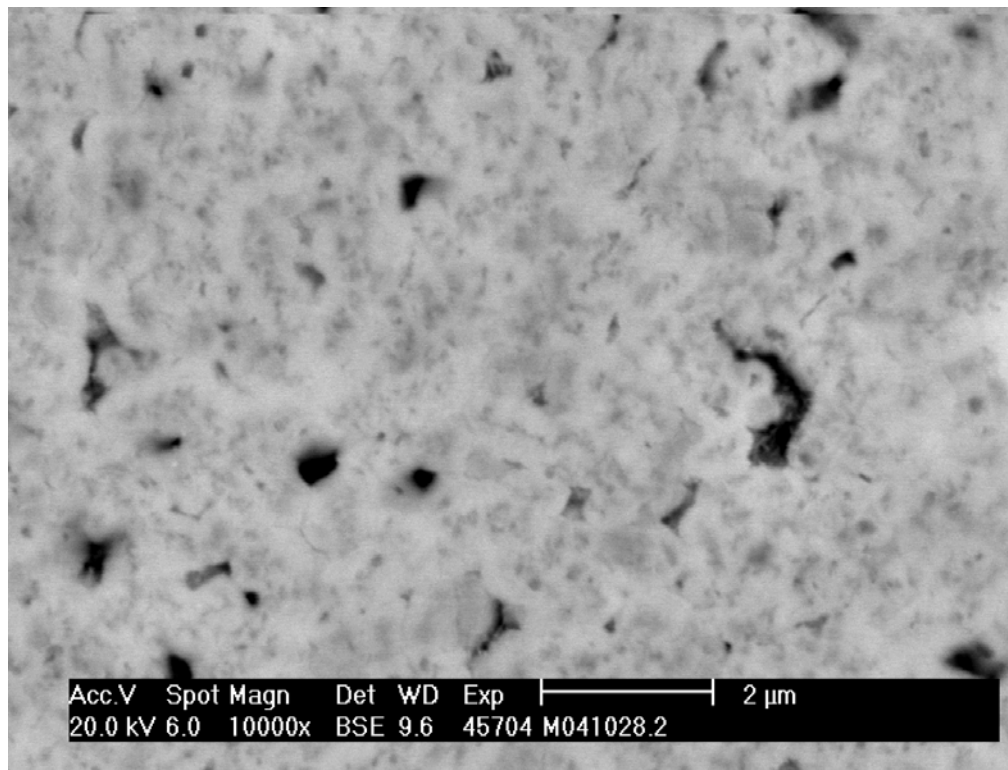**Figure 7-4:** IPyC layer of ZrO2-500-AK2 (secondary electron image).

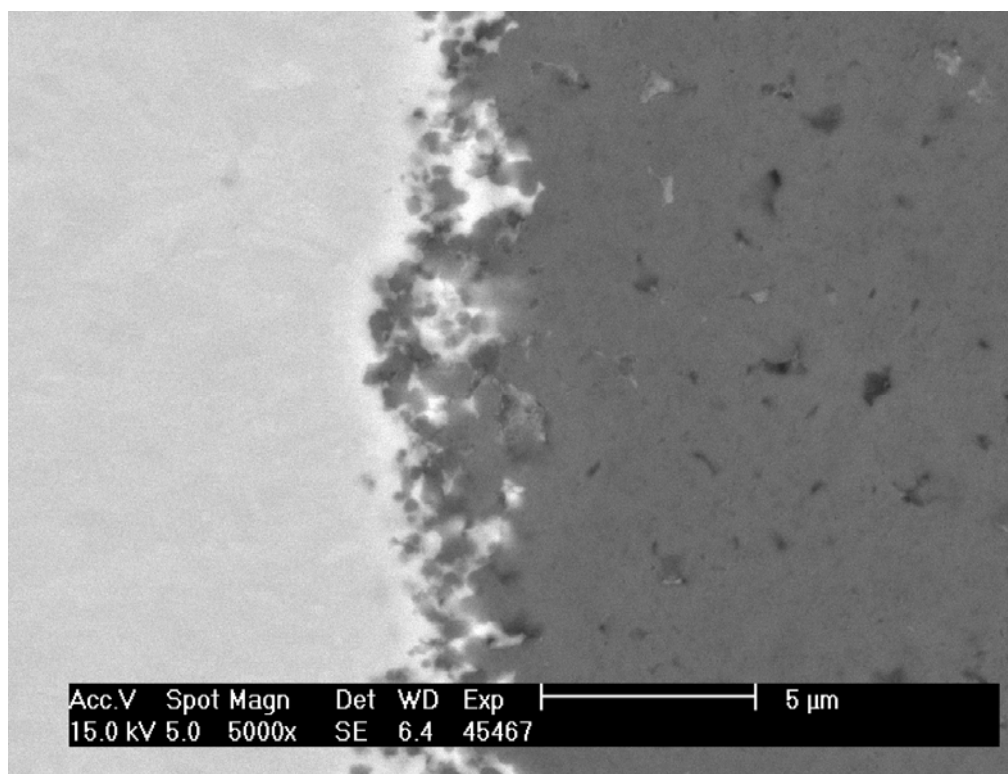**Figure 7-5:** IPyC layer of ZrO2-500-AK2 (backscatter electron image).

Figure 7-6: IPyC/SiC interface from ZrO2-500-AK2 (SiC on left; secondary electron image).
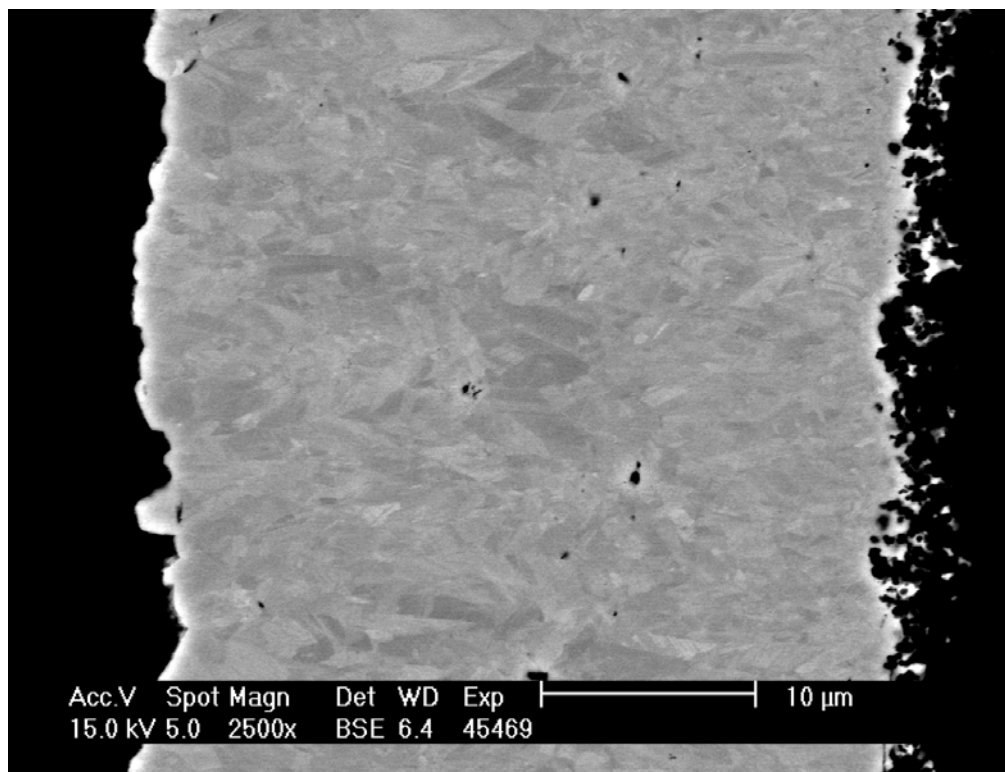
Figure 7-7: SiC layer of ZrO2-500-AK2 (backscatter electron image). Note the difference between the IPyC/SiC interface (right boundary) and the OPyC/SiC interface (left boundary).
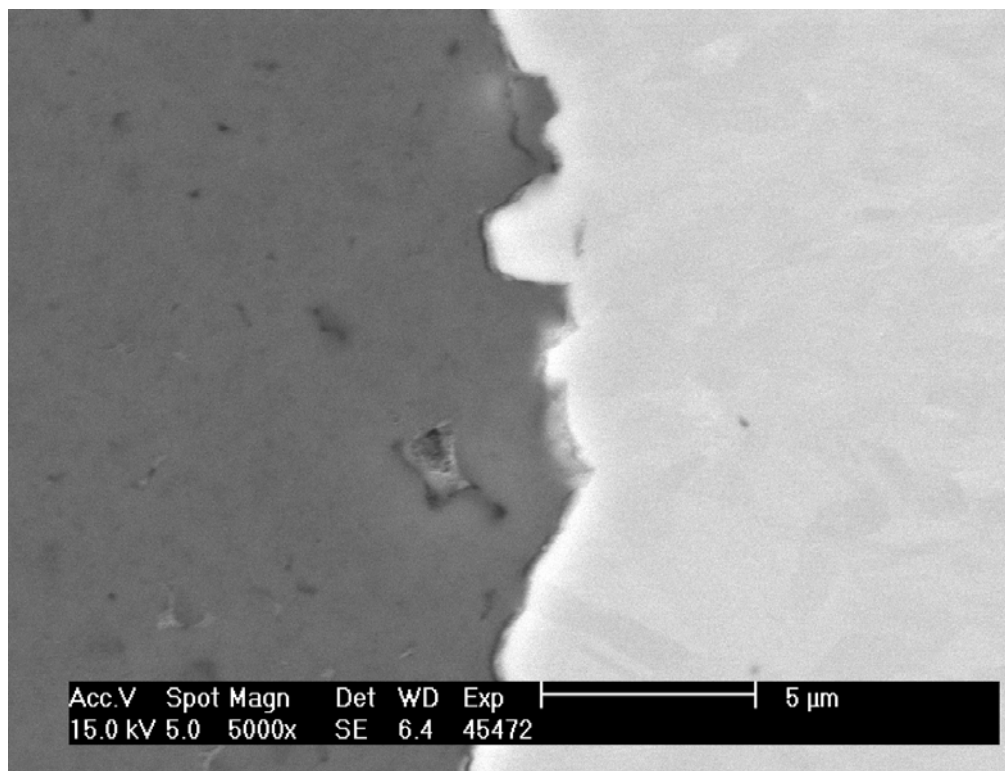

Figure 7-8: SiC/OPyC interface from ZrO2-500-AK2 (SiC on right; secondary electron image).
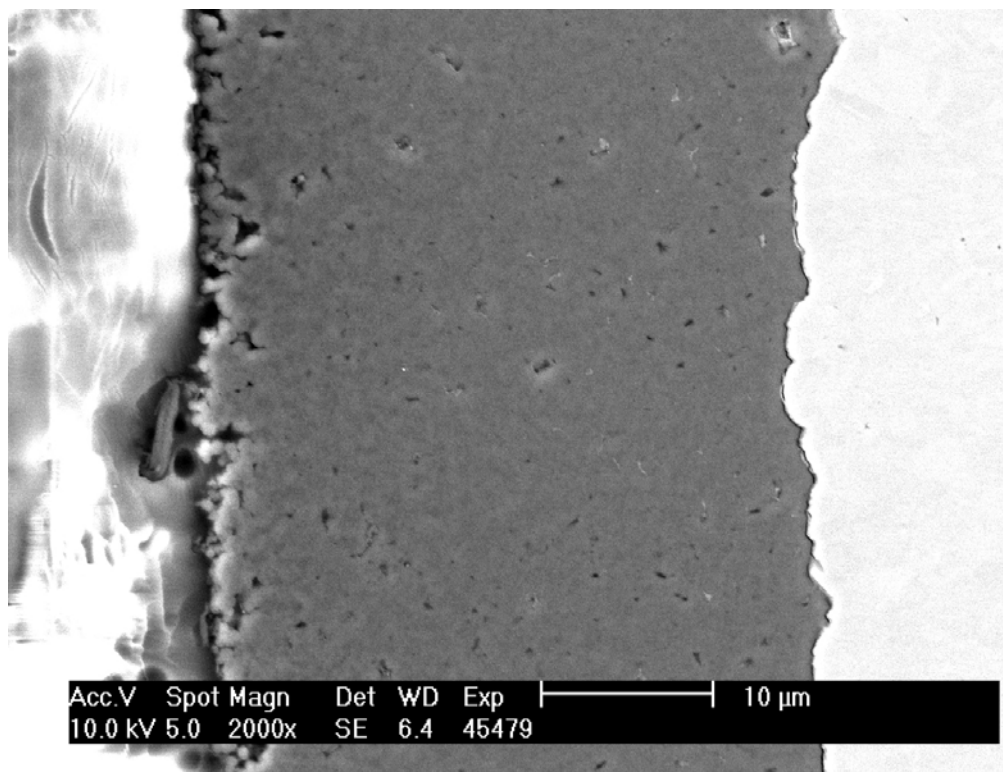
Figure 7-9: OPyC layer of ZrO2-500-AK2 (secondary electron image; SiC layer to the right).

7.2 Grain size of SiC layer

The grain size of the SiC layer was determined using ASTM standard E112-96. Grain boundaries were manually identified from SEM micrographs of the SiC layer. The ASTM grain size number, the grain number per square millimeter, and average grain area were approximated using a planimetric (Jeffrie's) procedure with a rectangular window (Figure 7-10 & Figure 7-11). Grain boundary identification for fine-grained SiC was subjective, so all results should be taken as approximate descriptions of the SiC microstructure.

Table 7-1 summarizes the grain size results for the two micrographs of ZrO2-500-AK2 and the one micrograph of the German reference fuel. Data from German reference fuel were included for comparison. SiC grains near the IPyC/SiC interface were too small and indistinct to delineate for ZrO2-500-AK2. The grain sizes for ZrO2-500-AK2 and the German reference fuel were comparable.
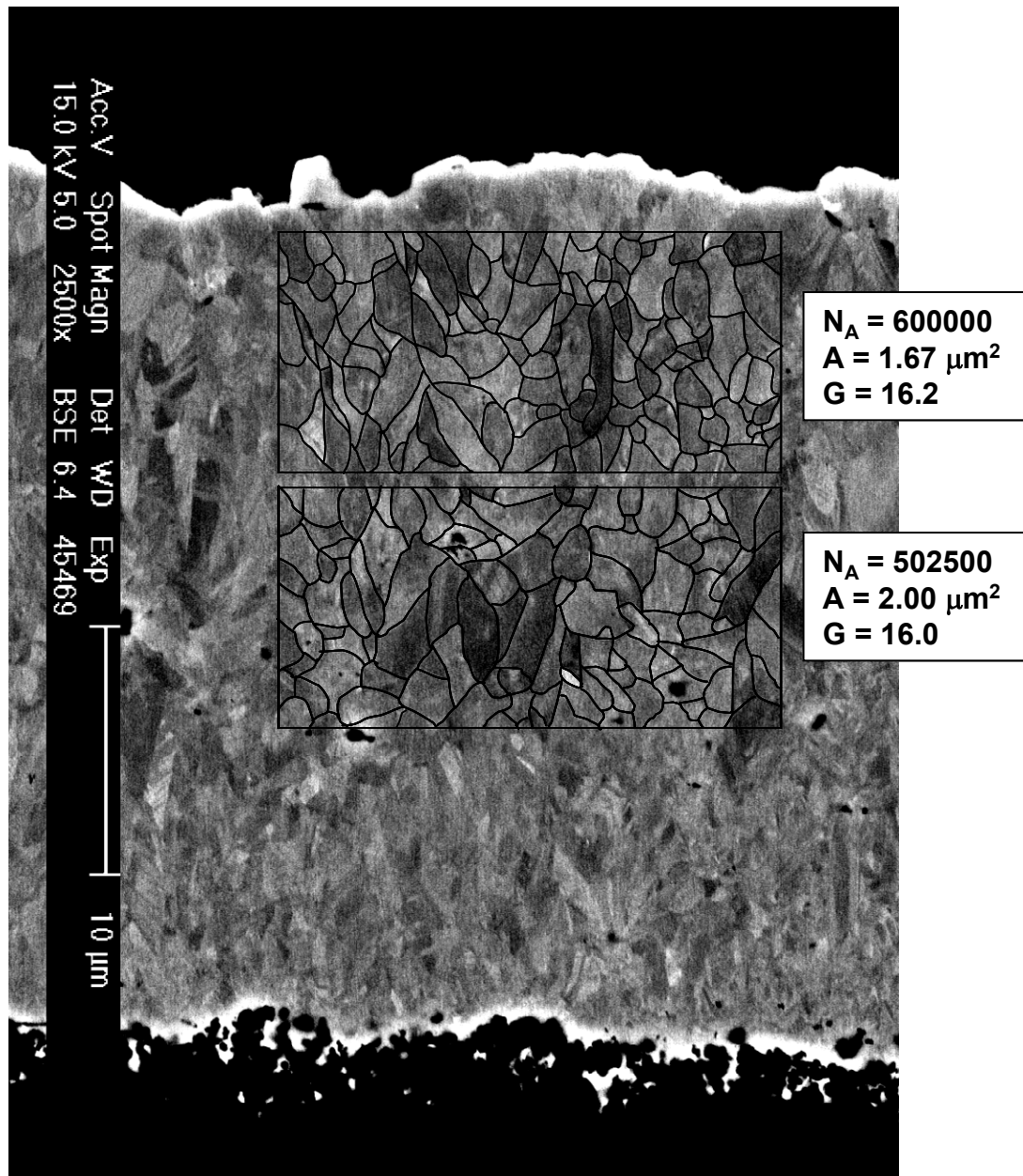
Figure 7-10: Grain size identification for ZrO2-500-AK2 at outer and middle regions of SiC layer. Grains in the inner region (close to IPyC) were too small and indistinct to reliably indentify. Image #45469.
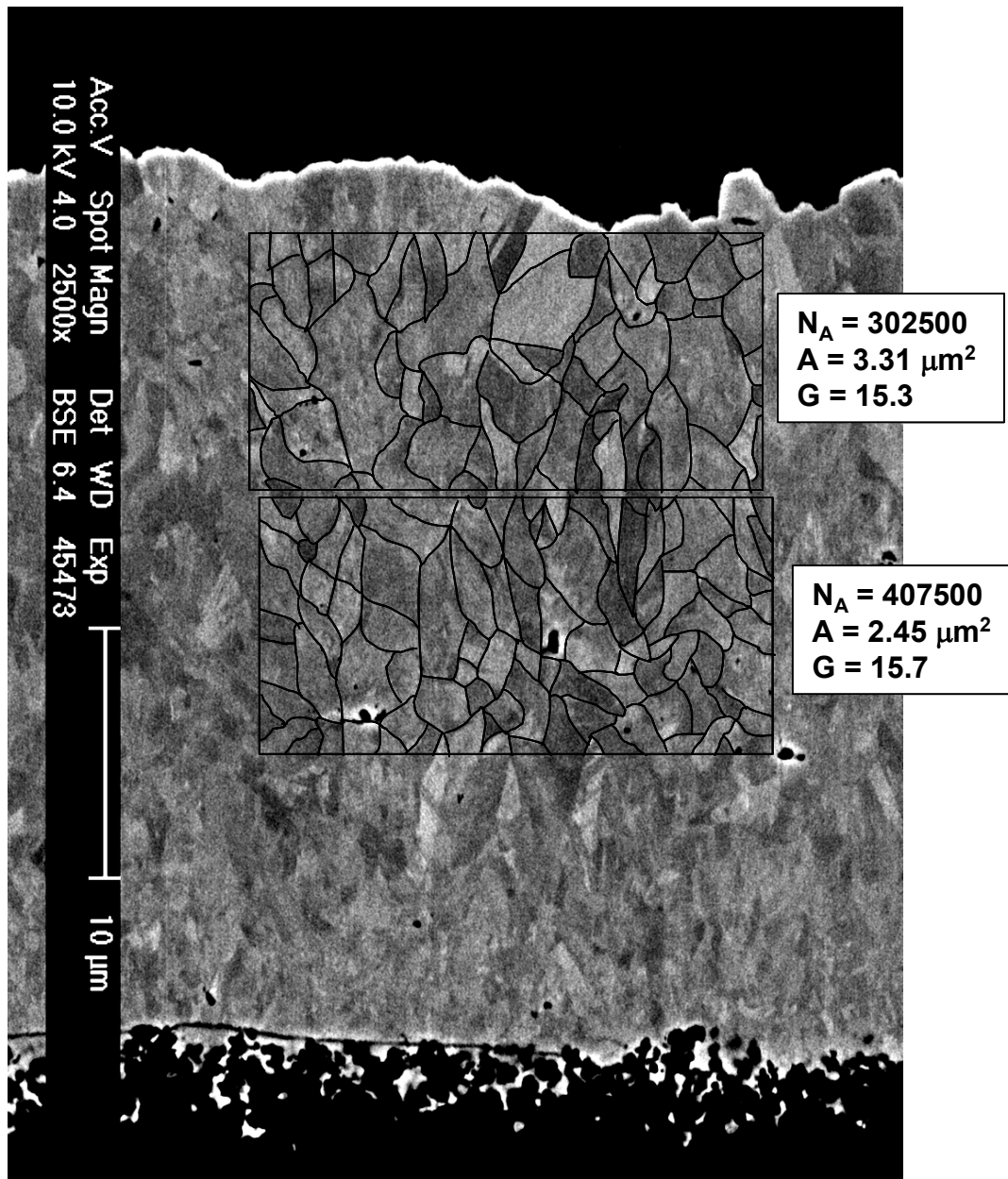
Figure 7-11: Grain size identification for ZrO2-500-AK2 at outer and middle regions of SiC layer. Grains in the inner region (close to IPyC) were too small and indistinct to reliably indentify. Image #45473.
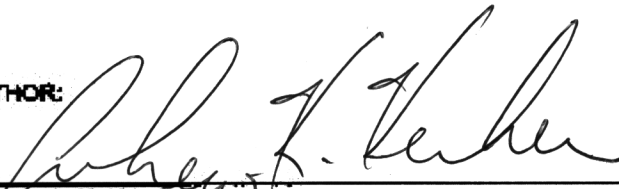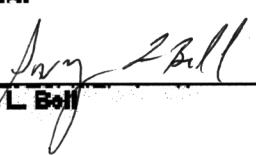
Table 7-1: Results from SiC grain size analysis

	Measured Area	ASTM Grain Size #, G	Grain number, N_A (mm^{-2})	Ave. Grain Area, A (μm^2)
AGR-06 Reference (German reference fuel)	Outer area of SiC layer	15.4	335000	2.99
	Middle of SiC layer	15.2	287500	3.48
	Inner area of SiC layer	15.4	342500	2.92
ZrO$_2$-500-AK2 (Image #45469)	Outer	**16.2**	**600000**	**1.67**
	Middle	**16.0**	**502500**	**2.00**
	Inner	-	-	-
ZrO$_2$-500-AK2 (Image #45473)	Outer	**15.3**	**302500**	**3.31**
	Middle	**15.7**	**407500**	**2.45**
	Inner	-	-	-

ADVANCED GAS REACTOR PROGRAM
OAK RIDGE NATIONAL LABORATORY

ORNL DOCUMENT CLEARANCE / REGISTRATION FORM

PERSON PREPARING FORM: Karen Y. Fugate	PHONE NO.: 576-7054	DATE SUBMITTED: June 08, 2005
DOCUMENT NO.: ORNL/CF-05/12	SPONSOR: DOE-NE / Dr. Madeline Feltus	
TITLE: Results from ORNL Characterization of ZrO2-500-AK2 — Surrogate TRISO Material		
AUTHOR(s): Andrew K. Kercher and John D. Hunn		
SIGNATURES: AUTHOR: Name: A. K. Kercher		June 13, 2005 Date
TECHNICAL REVIEWER: Name: O. M. Stansfield		June 10, 2005 Date
APPROVER: Name: G. L. Bell		6-10-05 JH for GLB Date